UNIVERSITY OF LATVIA

FACULTY OF PHYSICS, MATHEMATICS AND OPTOMETRY

KEVON KADIWALA

Exploring Novel Synthesis Methods For Transition Metal Dichalcogenides and Investigating Their Properties

SUMMARY OF DOCTORAL THESIS

Submitted for the Doctoral degree in Physics

Subfield of Materials Physics

Scientific Advisor:

Dr. phys. Boris Polyakov

RIGA, 2024

The doctoral thesis work was carried out in Institute of Solid State Physics, University of Latvia from 2020 to 2024.

The thesis contains an introduction, 5 chapters and a reference list.

Form of the thesis: dissertation in materials physics

Supervisor: *Dr. phys.* **Boris Polyakov**, senior researcher

Reviewers:

1. _____
2. _____
3. _____

The thesis will be defended at the public session of the Doctoral Committee of Physics, Astronomy and Mechanics of University of Latvia on _____ in _____.

The thesis is available at the Library of the University of Latvia, Raiņa bulv. 19.

Chairman of the Doctoral Committee

Secretary of the Doctoral Committee

Abstract

The field of Transition Metal Dichalcogenides (TMDs) has gathered significant attention due to its promising applications in electronics, optoelectronics, catalysis, and more. However, the current challenge lies in achieving scalable growth that meets commercial demands. This bottleneck has impeded the widespread commercialization of TMD-based products and necessitates a concerted effort to develop synthesis techniques that are both efficient and reproducible. This work seeks to address this critical issue by exploring a range of unique synthesis approaches designed to overcome these limitations.

The primary objective here, is to establish innovative methodologies for synthesizing TMD thin films on large-area substrates, ensuring consistency in geometry, quality, and reproducibility. Pulsed Laser Deposition (PLD) is one such method, offering precise control over film thickness and composition. Its versatility makes it suitable for scalable growth and the creation of heterostructures, enhancing device performance. Additionally, the combination of magnetron sputtering and chemical vapor transport (CVT) offers another promising approach. Magnetron sputtering allows precise deposition of precursor materials, while CVT enables controlled selenization or sulfurization for high-quality films. Ampoule-assisted conversion adds flexibility by providing a vacuum-sealed environment, reducing defects and improving crystallinity.

Beyond synthesis, this work delves into the detailed characterization of the synthesized TMD materials to evaluate their properties. Techniques like X-ray diffraction, Raman spectroscopy, and electron microscopy are employed to examine the films' chemical and structural properties, while electrical and optical analyses assess their quality for potential applications. By understanding the mechanisms of TMD synthesis and leveraging their unique properties, this research aims to facilitate broader adoption of TMD-based technologies. The findings could lead to breakthroughs in flexible electronics, high-performance transistors, and advanced photodetectors, ultimately driving innovation and enabling new commercial applications which have a lasting impact on technology and society.

Keywords: Transition Metal Dichalcogenides, Thin Films, Pulsed Laser Deposition, Magnetron Sputtering, Chemical Vapor Transport

Table of Contents

List of abbreviations

AFM: Atomic Force Microscopy

ALD: Atomic Layer Deposition

CDW: Charge Density Wave

CVD: Chemical Vapour Deposition

CVT: Chemical Vapour Transport

DC: Direct Current

DFT: Density Functional Theory

DIW: Deionized Water

EDX: Energy Dispersive X-ray Spectroscopy

HER: Hydrogen Evolution Reaction

h-BN: Hexagonal Boron Nitride

ICDD: International Centre for Diffraction Data

MOCVD: Metal Organic Chemical Vapour Deposition

μm: Micrometre

nm: Nanometre

NWs: Nanowires

PDF: Powder Diffraction File

PLD: Pulsed Laser Deposition

Q-switching: Quality-switching (in lasers)

SEM: Scanning Electron Microscopy

TEM: Transmission Electron Microscopy

TMD: Transition Metal Dichalcogenide

XPS: X-ray Photoelectron Spectroscopy

XRD: X-ray Diffraction

1D: One-Dimensional

2D: Two-Dimensional

1. Introduction

Transition metal dichalcogenides (TMDs) have emerged as a prominent class of materials within the field of materials science, captivating researchers due to their unique properties and diverse potential applications[1–5]. Characterized by a layered structure wherein transition metal atoms are covalently bonded between chalcogen atom layers arranged in a hexagonal lattice, TMDs exhibit remarkable tunability[2,6–9]. This tunability stems from the ability to manipulate factors such as layer thickness, chemical composition, and the application of external stimuli like strain and doping. By meticulously controlling these parameters, researchers can engineer the electronic, optical, mechanical, and catalytic properties of TMD materials with high precision[10–14]. This exceptional degree of control positions TMDs as highly attractive candidates for a wide range of applications across various scientific disciplines[4,9,14–17].

In the domain of electronics, TMDs have attracted significant attention as promising materials for next-generation electronic devices. Their inherent advantages include high carrier mobility, excellent electrostatic control, and compatibility with flexible and transparent substrates – all crucial characteristics for the development of advanced electronics[18,19]. Field-effect transistors (FETs) fabricated using TMDs have demonstrated impressive performance metrics, signifying their potential utility in logic circuits, memory devices, and beyond[5,18,20–26]. Furthermore, the creation of TMD heterostructures – achieved by stacking different TMD layers or combining TMDs with complementary materials like graphene or boron nitride – offers the exciting possibility of realizing entirely novel electronic functionalities and device architectures[1,2,16].

TMDs also hold immense promise in the realm of optoelectronics due to their intriguing optical properties. These properties encompass strong light-matter interactions, tuneable bandgaps, and efficient light emission. By harnessing these attributes, TMDs are being explored for applications in photodetectors, light-emitting diodes (LEDs), and photovoltaic devices[27–29]. By leveraging the unique quantum confinement effects and excitonic phenomena observed in TMD monolayers, researchers are actively developing ultra-compact photonic and optoelectronic devices boasting unprecedented performance characteristics[30–34]. These advancements pave the way for the realization of integrated photonic circuits and quantum technologies. The potential of TMDs extends beyond electronics and optoelectronics. They are also demonstrating exceptional promise as efficient and Earth-abundant catalysts for various chemical reactions, including hydrogen evolution, oxygen reduction, and nitrogen fixation[6,24,35]. The high surface areas, abundant active sites, and tuneable electronic structures exhibited by TMD materials contribute to their

remarkable catalytic activity[14,36,37]. This has opened doors for their utilization in sustainable energy conversion technologies and environmental remediation efforts.

Furthermore, TMDs are making significant inroads in the field of energy storage and conversion, with potential applications in lithium-ion batteries, supercapacitors, and electrochemical water splitting[16,38–40]. Their high surface area, mechanical flexibility, and chemical stability make TMD-based electrodes and catalysts attractive candidates for enhancing the performance and longevity of energy storage and conversion devices. Finally, TMDs are proving to be exceptional sensing materials, exhibiting exceptional sensitivity to external stimuli such as gases, biomolecules, and mechanical strain[5,19,27,41]. By functionalizing TMD surfaces with specific ligands or exploiting their intrinsic electronic and optical responses, researchers are developing ultrasensitive and selective sensors capable of detecting a wide range of analytes. These sensors have the potential to revolutionize various fields, including environmental monitoring, healthcare diagnostics, and industrial process control[36,42–44]. The exploration of TMDs is an ongoing endeavour, and as researchers continue to unveil their secrets, we can anticipate even more groundbreaking discoveries that will significantly reshape various technological landscapes. This ongoing pursuit underscores the immense potential of TMDs and their transformative role in the future of materials science.

1.1 Objectives of this work

The primary goal of this work was to synthesize and explore transition metal dichalcogenides through diverse methodologies and subsequently analyse the resulting materials. By doing so, the aim was set for assessing both the potential applications of the synthesized materials and the effectiveness of the methodologies employed for their synthesis *(fig. 1.1)*. Following objectives give detailed understanding of what was intended to achieve through this study:

1. **Develop scalable synthesis methods** for fabricating thin films of TMDs on various substrates, including one-dimensional nanowires and two-dimensional silicon or sapphire wafers, to enable large-scale applications of these materials.
2. Develop synthesis techniques for TMDs using their respective transition **metals as precursors instead of their oxides**, which often have high thermal stability. For instance, using Ta metal instead of Ta_2O_5 to produce $TaSe_2$ can be a more effective approach due to the challenges associated with the thermal stability of Ta_2O_5.

3. **Synthesize a select few TMDs from their respective metal and metal oxide precursors** under similar conditions to study the electrical properties and morphological differences, and identify potential applications based on these findings.
4. Use characterization techniques such as XRD, Raman, XPS to study

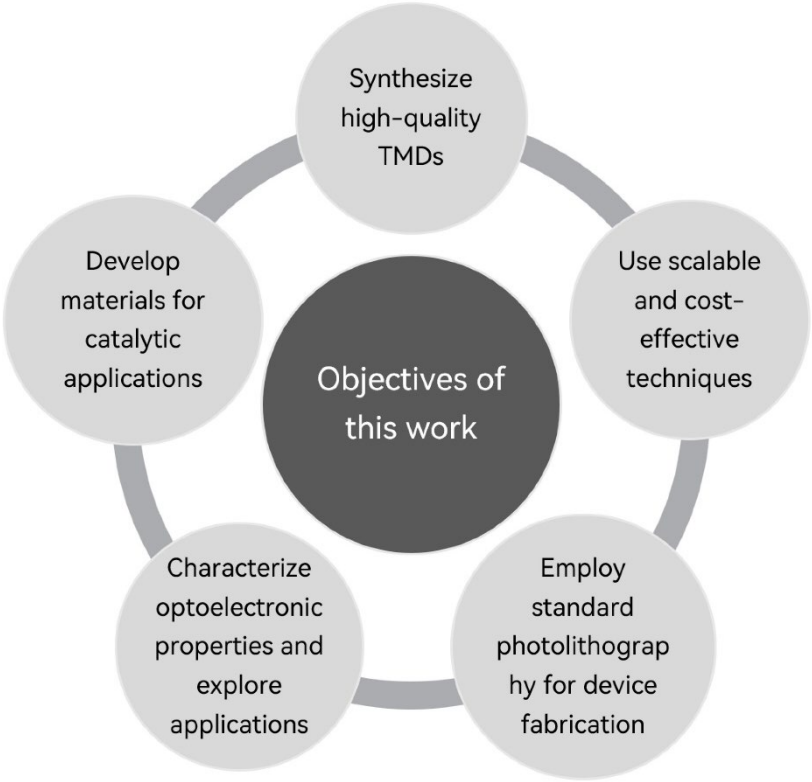

Figure 1.1: Directions of the desired results of this study to be obtained as the outcomes of this work.

the chemical and structural properties of the produced materials in addition to SEM, TEM, AFM for more deeper understanding, **exploring their potential applications** in various fields.
5. Showcase the **use of standard photolithography and control the geometry** of the produced TMD thin films to demonstrate the possible device fabrication as part of this methodology and its usability in various applications (e.g. photosensors).

All the research described in this dissertation was carried out in Institute of Solid State Physics of University of Latvia.

1.2 Scientific novelty

The research results presented in this thesis hold scientific significance and have been published in various international journals. To point the key novelties of the presented work here, following list is prepared:

- ***Comparison of two synthesis methodologies for growing GaN-MoS_2 and GaN-WS_2 core-shell nanowires:*** The study explored two different methods for fabricating GaN-based core-shell nanowires, showing that by adjusting process parameters, it is possible to achieve uniform or island-like coatings with potential applications in energy and as photocatalysts for hydrogen production.
- ***Developed a robust method for fabricating core/shell nanowires with 2D TMD shells:*** This study presents a scalable four-step process for fabricating core/shell nanowires with a well-defined $TaSe_2$ shell, using a vacuum-sealed selenium atmosphere, demonstrating that this technique is versatile and applicable to a wide range of 2D chalcogenides.
- ***First-time comparison of WSe_2 films from WO_3 and W metal precursors:*** This work compared the characteristics of WSe_2 thin films synthesized from two distinct precursors, revealing that WO_3-based films generally had higher photocurrent and stability compared to those from W metal, suggesting that WO_3 is a more effective precursor for the CVT synthesis of WSe_2.
- ***First-time comparison of $ReSe_2$ films from Re metal and ReO_x precursors:*** The study introduced a novel method for $ReSe_2$ synthesis using atmospheric pressure CVT, showing significant differences in surface morphology based on precursor material and demonstrating potential for various applications, including non-linear optics.
- ***Developed a unique synthesis method for $TiSe_2$ and VSe_2 thin films with a 2-step process:*** This study used a scalable approach for the large-area synthesis of $TiSe_2$ and VSe_2 thin films, showing that both materials retained their continuity after selenization. This method provides opportunities to create continuous films on a large scale, with broader applications and extension to other TMDs.

1.3 Outline of this work

This work delves into the exciting realm of Transition Metal Dichalcogenides (TMDs), a class of materials with immense potential for next-generation electronics and optoelectronics. We begin by exploring the current state of the field and the key objectives driving our research (Chapter 1). We then clearly outline the objectives of our research, emphasizing the scientific novelty brought by our approach.

Chapter 2 lays the groundwork by providing a fundamental understanding of TMDs and delves into various synthesis techniques employed for their fabrication in this work and to explore what concepts they were utilized. Chapter 3 focuses on the creation of heterostructures – novel structures combining different TMDs – with a specific emphasis on MoS_2/WS_2 grown on GaN nanowires and $TaSe_2$ grown on ZnS nanowires with an intermediary layer (Chapter 3.1-3.2). This chapter concludes by discussing the key results and their potential implications. Chapter 4 explores the growth of individual TMD thin films, investigating materials such as WSe_2, $ReSe_2$, $TiSe_2$, and VSe_2 (Chapter 4.1-4.3). Here, we detail the specific synthesis processes employed and present the key findings associated with each study.

Finally, Chapter 5 serves as a comprehensive summary, revisiting the initial objectives and evaluating our success in achieving them. Chapter 6 concisely presents the main theses of the work, providing a clear takeaway for the reader.

This work offers valuable insights into the synthesis of various TMD materials and heterostructures, paving the way for further exploration of their potential in advanced technological applications.

2. General topics

2.1 Fundamentals of Transition Metal Dichalcogenides

Transition metal dichalcogenides are a class of materials composed of layers of transition metal atoms sandwiched between layers of chalcogen atoms (sulphur, selenium, or tellurium) [45,46]. This unique layered structure imparts TMDs with a distinctive set of properties that have garnered significant attention in recent years [47–50]. The fundamental building block of TMDs is a single layer, often referred to as a monolayer. The weak van der Waals forces between these layers provide TMDs with their characteristic flexibility and ability to be exfoliated into individual layers. This layered structure is responsible for many of the remarkable properties exhibited by TMDs, including their exceptional mechanical flexibility, high surface area, and anisotropic electrical and optical properties [51–54].

Understanding the interplay between layered structure and lattice matching is essential for the rational design and fabrication of TMD-based devices. By carefully selecting materials with compatible lattice parameters and controlling the growth conditions, it is possible to create high-quality heterostructures with desired properties [55–58]. As research in this field continues to advance, we can expect to see even more exciting developments in the field of TMD-based materials and devices. Below are some of the fundamental properties of the TMDs synthesized in this research:

- MoS_2 (Molybdenum Disulfide): Hexagonal crystal system (P63/mmc) *(fig. 2.1)*, lattice parameters a = 3. 161 Å, c = 12.295 Å, formation energy -1.09 eV/atom, density 5.06 g/cm^3. Known for electronic and optoelectronic applications. 2H phase is most stable.
- WS_2 (Tungsten Disulfide): Hexagonal crystal system (P63/mmc), lattice parameters a = 3.153 Å, c = 12.32 Å, formation energy -1.13 eV/atom, density 7.54 g/cm^3. Notable for electronics and catalysis. 2H phase is most stable.
- $TaSe_2$ (Tantalum Diselenide): Hexagonal crystal system (P63/mmc), lattice parameters a = 3.434 Å, c = 12.706 Å, formation energy -0.80 eV/atom, density 9.16 g/cm^3. Known for superconducting properties. 2H phase is more stable at room temperature.
- WSe_2 (Tungsten Diselenide): Hexagonal crystal system (P63/mmc), lattice parameters a = 3.288 Å, c = 12.96 Å, formation energy -1.03 eV/atom, density 9.32 g/cm^3. Used in electronics and optoelectronics. 2H phase is most stable.
- $ReSe_2$ (Rhenium Diselenide): Triclinic crystal system (P-1) *(fig. 2.1)*, lattice parameters a = 6.732 Å, b = 6.609 Å, c = 6.626 Å, formation energy

-0.91 eV/atom, density 7.33 g/cm^3. Known for anisotropic properties. Triclinic phase is most stable.

- $TiSe_2$ (Titanium Diselenide): Hexagonal crystal system (P-3m1) *(fig. 2.1)*, lattice parameters a = 3.538 Å, c = 6.008 Å, formation energy -0.80 eV/atom, density 4.95 g/cm^3. Known for charge density wave properties. 1T phase is most stable.

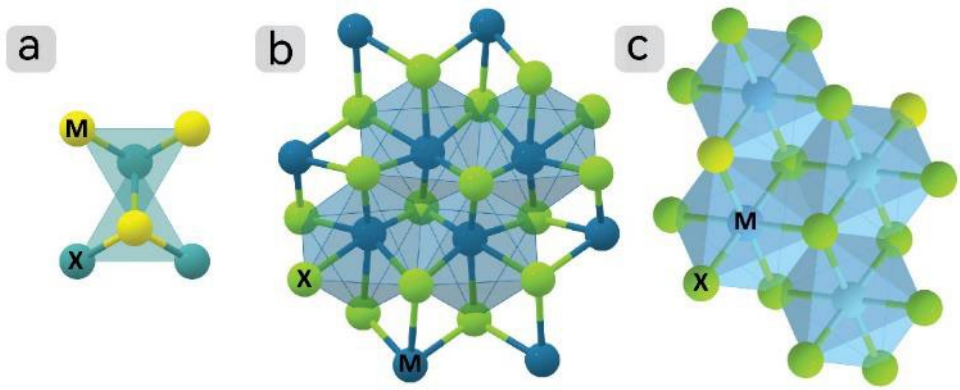

Figure 2.1: Graphical crystal structures of (a) hexagonal structure with a space group of P6$_3$/mmc (b) triclinic crystal system with a space group of P-1 and (c) hexagonal crystal structure with a space group of P-3m1 where M represents atoms of Transition metals and X represents Chalcogen group atoms (S, Se). [80]

- VSe_2 (Vanadium Diselenide): Hexagonal crystal system (P-3m1), lattice parameters a = 3.356 Å, c = 6.108 Å, formation energy -0.67 eV/atom, density 5.81 g/cm^3. Potential use in energy storage and electronics. 1T phase is most stable.

The versatility of TMDs in responding to external stimuli underscores their potential as a platform for groundbreaking advancements in electronics and optoelectronics. As research in this field progresses, the development of increasingly sophisticated devices that leverage the unique electrical properties of these remarkable materials can be expected.

2.2 Common Synthesis Techniques Overview

From a variety of synthesis techniques for TMDs, a brief summary of each used technique in this work is discussed from their fundamental working to their usage *(fig. 2.2)*.

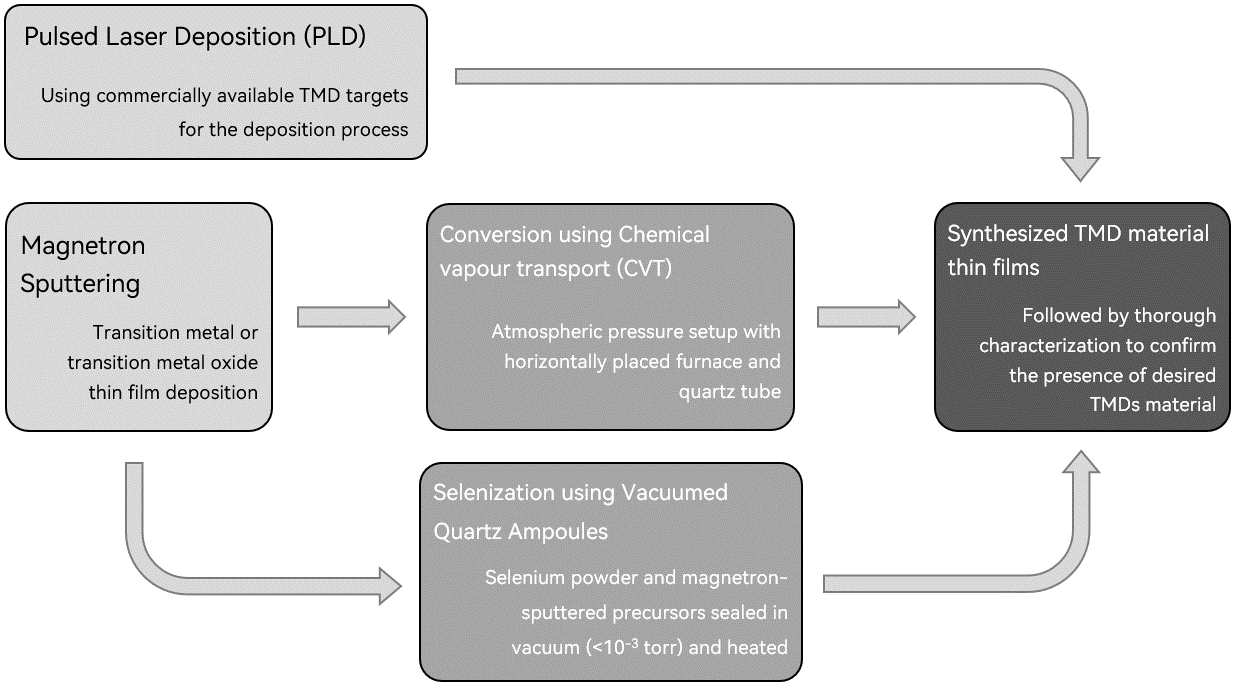

Figure 2.2: Flow chart of the three different methodologies consisting of at times more than one technique for the synthesis of TMDs films (left to right) in this work.

Pulsed laser deposition (PLD) is an advanced thin film deposition technique used extensively for producing high-quality films of various materials, including transition metals and their oxides. This process utilizes high-power laser pulses to ablate material from a target, which then deposits onto a substrate to form a thin film. PLD is known for its ability to precisely control film composition and structure, making it ideal for complex materials and heterostructures [59,60]. The PLD process begins with selecting a target material, typically a high-purity transition metal or metal oxide. The target is placed in a vacuum chamber, which is then evacuated to achieve a low-pressure environment, often with a background gas such as oxygen for oxide films. A high-energy laser, usually an excimer or Nd:YAG laser, is directed through a window into the chamber, where it focuses onto the target material. The laser pulses ablate the target, creating a plume of ejected material that travels towards the substrate. The substrate is positioned opposite the target, and its temperature can be controlled to influence the film's properties. As the ablated material condenses on the substrate, it forms a thin film with characteristics that can be precisely tailored by adjusting the laser parameters, such as energy, frequency, and pulse duration.

In summary, pulsed laser deposition is a powerful technique for creating high-quality thin films of transition metals and their oxides. By utilizing high-power laser pulses to ablate target materials in a controlled environment, PLD enables precise control over film composition and structure. This method is

essential for producing advanced materials with tailored properties for a wide range of technological applications.

Magnetron sputtering is a versatile technique used for the deposition of thin films, particularly for transition metals and their oxides. This process involves ejecting material from a target using energetic ions generated in a plasma, which then deposit onto a substrate to form a thin film. Magnetron sputtering can be performed in either direct current (DC) or radio frequency (RF) modes, with DC sputtering being especially suitable for conductive materials like transition metals [61,62]. Magnetron sputtering is a critical technique for depositing transition metals and their oxides. It involves sputtering material from a target in a controlled vacuum environment, allowing precise control over film properties. This method is integral to producing thin films for a wide range of advanced applications.

Chemical vapor deposition (CVD) has emerged as a powerful technique for synthesizing atomically thin transition metal dichalcogenide (TMD) crystals with precise control over their thickness, crystallinity, and morphology. In this process, precursor gases containing transition metal and chalcogen species react on a heated substrate, forming TMD thin films. To enhance the CVD synthesis of atomically thin TMD crystals, researchers have explored the use of salt as an additive. Rather than acting as a seed for crystal growth, salt serves to lower the energy required for the reaction between metal oxides and chalcogen species, thereby improving crystal growth. This enhancement occurs by increasing the partial pressure of TMD vapor at a given temperature [63,64]. CVD offers a versatile and scalable approach for synthesizing atomically thin TMD crystals. The addition of salt as an additive in precursor mixtures can enhance crystal growth by reducing the energy barrier for reaction. By carefully controlling precursor chemistry, growth parameters, and substrate properties, researchers can achieve precise control over TMD crystal growth and tailor their properties for various applications.

Quartz ampoule fabrication plays a crucial role in the synthesis of various materials, typically made of high-purity quartz glass, provide a sealed environment for conducting high-temperature reactions under controlled conditions [65]. These ampoules are used to house precursor materials and facilitate their conversion into TMD thin films through processes such as selenization or sulfurization. The fabrication of quartz ampoules involves several steps to ensure their integrity and functionality for high-temperature reactions. First, high-quality quartz glass tubes are selected based on purity and thermal stability. These tubes are then cut to the desired length and cleaned thoroughly to remove any contaminants that could affect the reaction process. Next, the ampoules are sealed using a high-temperature torch or a specialized sealing machine to create a hermetic seal that prevents leakage of gases and maintains a controlled environment inside the ampoule during the reaction

process*)*. In the synthesis of TMD thin films, quartz ampoules serve as reaction vessels for housing precursor materials and facilitating their conversion into TMDs through controlled thermal processes. Quartz ampoule fabrication is a crucial technique for the synthesis of TMD thin films through processes such as selenization or sulfurization. By combining techniques such as magnetron sputtering for precursor deposition with ampoule heating in a high-temperature furnace, researchers can control the conversion of precursor materials into TMDs under vacuum conditions with high partial pressures of Se/S vapor. This approach enables the production of high-quality TMD thin films with tailored properties for a wide range of applications in electronics, optoelectronics, catalysis, and beyond.

2.3 Material synthesis and investigation details

GaN nanowires and MoS_2/WS_2 shell synthesis: GaN NWs were synthesized via atmospheric pressure chemical vapour transport method in a horizontal quartz tube reactor. 2 g metallic Ga (99.999%, Alfa Aeasar) was loaded in a ceramic boat and placed in the centre of the quartz tube, oxidized silicon wafers SiO_2/Si (100) (Semiconductor Wafer, Inc.) coated with spherical Au nanoparticles (NPs, Alfa Aesar, water suspension, 100nm diameter) were placed downstream in a lower temperature region. Au NPs were used as a catalyst for the vapour-liquid–solid (VLS)mechanism. The reactor was heated to 940°C under a flow of carrier gas mixture Ar/H_2-35%, then gaseous NH_3 flow in 1:1 ratio to the carrier gas was introduced and maintained for 30 min for the gas-phase reaction and NW growth, followed by natural cooling to the room temperature under Ar/H_2 flow. As a result, 5–20 μm long GaN NWs were produced on the SiO_2/Si substrate. Few-layers of MoS_2 and WS_2 on GaN NWs were obtained with two different routes. The first route consists of two steps – deposition of amorphous MoO_3 and WO_3 coating on GaN NWs via reactive DC magnetron sputtering of a metallic target in a mixed Ar/O_2 atmosphere, followed by subsequent sulfurization of the samples in a quartz tube reactor at high temperatures. The optimal sacrificial precursor film thickness (on a flat substrate) was found to be 30 nm and 40 nm for MoO_3 and WO_3, respectively. Optimal sulfurization temperature was 750°C for MoS_2 and 800°C for WS_2 coatings. The second route was pulsed laser deposition (PLD) from stoichiometric MoS_2 and WS_2 targets. 500 mJ 248 nm KrF laser beam was used for target ablation at 10Hz repetition frequency and 10^{-5} Torr background pressure. A few-layer MoS_2 coating was obtained with 1500 pulses at 600°C substrate temperature, and WS_2 coating with 3000 pulses at 650°C substrate temperature.

ZnS nanowires and Al_2O_3-$TaSe_2$ shell synthesis: Zinc sulphide (ZnS) nanowires (NWs) were synthesized on oxidized silicon (Si/SiO_2) substrates

(Semiconductor Wafer, Inc., Hsinchu, Taiwan) using a vapor-liquid-solid (VLS) growth mechanism. Gold nanoparticles (50 nm in diameter) (BBI International, Grand Forks, ND, USA) served as catalysts for the growth process. ZnS powder (0.4 g, >97%, Sigma Aldrich, St. Louis, MO, USA) was thermally sublimated at 950°C in a quartz tube reactor, and the resulting vapor was carried by an Ar/H_2-5% gas mixture to the substrate. Subsequently, an aluminium oxide (Al_2O_3) layer, approximately 6 nm thick, was deposited on the ZnS NWs using atomic layer deposition (ALD) at 150°C in a Savannah S100 reactor. Trimethylaluminum (TMA) and H_2O were used as precursors, with N_2 serving as the carrier gas. A thin layer of tantalum (Ta), approximately 15 nm thick, was deposited onto the ZnS/Al_2O_3 NWs using direct current (DC) magnetron sputtering from a Ta target (GoodFellow, Huntingdon, UK) in an argon atmosphere. Finally, the coated NWs were annealed in a selenium environment at 650 °C to transform the Ta layer into tantalum diselenide ($TaSe_2$). The annealing process was conducted in a vacuum-sealed quartz ampoule containing selenium pellets (50 mg, Sigma Aldrich) and Ta foil (100 mg, GoodFellow, Huntingdon, UK) to maintain a stable vapor pressure of $TaSe_2$ and minimize the vapor's transport to cooler areas of the ampoule.

Tungsten diselenide film synthesis: Sacrificial precursor films with varying thicknesses, from 3 nm to 50nm, were deposited on oxidized silicon wafers SiO_2/Si (100) (Semiconductor Wafer, Inc.) by reactive DC magnetron sputtering of a metallic tungsten target in a mixed Ar/O_2 atmosphere ($5\cdot10^{-3}$ torr, 30 sccm Ar, and 20 sccm O_2 gas flow at 300 W DC power). After the precursor material deposition, synthesis of WSe_2 was performed from W metal film and WO_3 film using CVT. The CVT setup consists of a horizontal open-end quartz tube reactor. For the procedure, selenium powder was loaded in a ceramic boat at one end of the quartz tube. The vapour of selenium was transported downstream to the W/WO_3 precursor material on a silicon substrate using the carrier gas mixture: Ar/H_2-5% in the case of WO_3 and 35% Ar/H_2 in the case of W. The temperatures (ranging from 600 to 850°C) were held constant for 20 min, followed by uninterrupted cooling to the room temperature.

Rhenium diselenide film synthesis: A two-step approach was employed, starting with the deposition of thin rhenium (Re) and rhenium oxide (ReO_x) films with thicknesses ranging between ~10 and 70 nm on substrates of a ~1 cm^2 square (cut by a diamond scriber) size at room temperature by reactive DC magnetron sputtering of a metallic rhenium target (99.9%) in an Ar or mixed Ar/O_2 (20 sccm: 10 sccm) atmosphere ($5\cdot10^{-3}$ torr, 100 W DC power). Prior to the magnetron deposition of the precursor thin films, the substrates underwent a cleaning process. This involved immersing them in an ultrasonic bath with acetone for 3 min, followed by a subsequent 3 min ultrasonic bath in deionized water (DIW). After the ultrasonic cleaning, the substrates were blow-dried using nitrogen (N_2) gas to ensure the removal of any residual contaminants.

These deposited precursor films served as the foundation for the subsequent conversion to $ReSe_2$ via CVT. The CVT setup was operated at atmospheric pressure using a 5% H_2/Ar gas mixture. The temperature range tested was from 550°C to 1000°C, with a process duration of 15 min (with a pre-heated furnace), and selenium powder (99.99%, Sigma Aldrich, St. Louis, MO, USA) placed at the intake end of the carrier gas. The furnace used here exhibited a temperature gradient, maintaining the target temperature primarily within the central 5 cm region, beyond which, the temperature decreased. Depending on the selected process temperature, the selenium powder was positioned in a zone where the temperature reached 350–400°C to facilitate its evaporation, to be carried by the flow of the carrier gas to placed samples.

Titanium and Vanadium diselenide film synthesis: Cleaned 10 mm^2 sapphire substrates (r-plane, Biotain Crystal Co.) were prepared using standard ultrasonic cleaning techniques with acetone and DI water. Thin films of Ti or V metal, approximately 15 nm thick, were deposited onto the cleaned substrates using DC magnetron sputtering in an argon atmosphere ($3 \cdot 10^{-3}$ torr, 30 sccm Ar, at 100 W DC power). The ampules were made from quartz tubes of 13 mm OD with 1 mm wall thickness and length of 120 ± 10 mm, were loaded with the metal-coated sapphire substrate, 50 mg of selenium powder, and 100 mg of grinded metal chips to absorb excess selenium. After lowering the pressure inside to $<10^{-3}$ torr, they were sealed and heated in a horizontal furnace at 650°C, 700°C, or 750°C for an hour, followed by rapid cooling to room temperature by exposing these ampoules to atmosphere.

Details of the investigative tools used:

- X-ray Diffraction (XRD): Rigaku MiniFlex 600 X-ray powder diffractometer with Cu Kα radiation (λ = 1.5406 Å). Rietveld analysis was performed using the BGMN program.
- X-ray Photoelectron Spectroscopy (XPS): ESCALAB Xi spectrometer from ThermoFisher with an Al Kα X-ray tube.
- Transmission Electron Microscopy (TEM): Tecnai GF20, FEI, operating at 200 kV.
- Scanning Electron Microscopy (SEM): Lyra, Tescan, and Helios 5 UX, Thermo Fisher Instruments.
- Energy Dispersive X-ray Spectroscopy (EDX): X-Max detector, SATW window.
- Optical Microscopy: Standard optical microscope.
- Atomic Force Microscopy (AFM): PARK NX10, Suwon, Korea.
- Hall Effect Measurement: HMS5000, Ecopia Hall Effect Measurement Systems.
- Spectrophotometry: Cary 7000 spectrophotometer, Agilent.
- Z-scan Measurement: ORPHEUS-HP + PHAROS PH2 femtosecond laser.

- Micro-Raman Spectroscopy: TriVista 777 confocal Raman system, Princeton Instruments.
- Photoresponse and I-V Measurements: Two-contact microprobe station, low-noise current preamplifier (SR570, Stanford Research Systems), oscilloscope (TDS2004B, Tektronix), and 405 nm semiconductor diode laser.

3. Producing Heterostructures with TMDs

3.1 MoS_2 and WS_2 grown on GaN nanowires

Experimental Method

This study focused on the synthesis of GaN-MoS_2 and GaN-WS_2 core-shell nanowires using two distinct methods *(fig. 3.1)*:

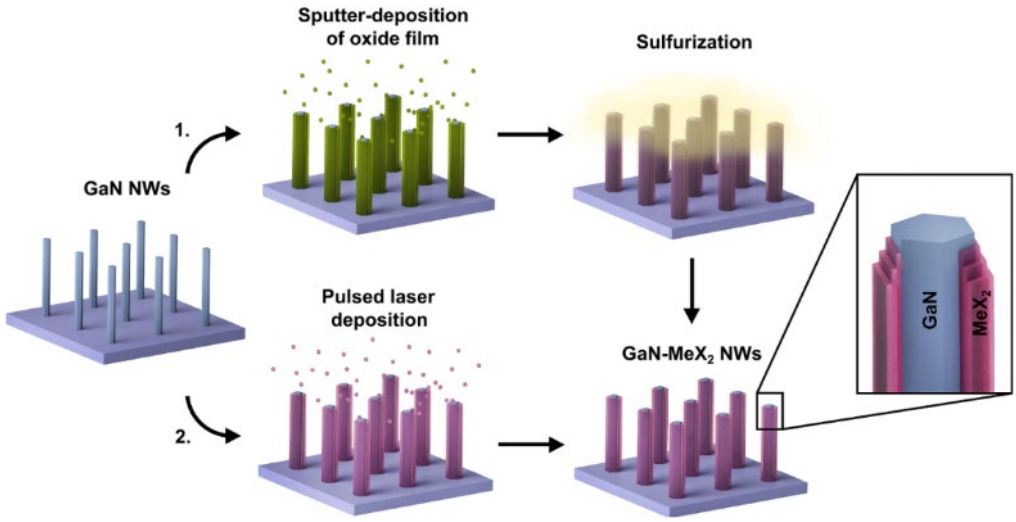

Figure 3.1: A schematic of both demonstrated GaN-MeX$_2$ core–shell NW preparation methods on Si/SiO$_2$ substrates: (1) two-step method, which includes sulfurization of pre-deposited metal oxide coating; and (2) direct deposition of MoS$_2$ or WS$_2$ with pulsed laser deposition

- Two-Step Process:
  i. Sputter-deposition of a sacrificial transition metal oxide coating (WO_3 or MoO_3) on GaN nanowires.
  ii. Sulfurization of the coated nanowires to convert the oxide into the corresponding sulphide (MoS_2 or WS_2).
- Pulsed Laser Deposition (PLD):

  Direct deposition of a few layers of MoS_2 or WS_2 onto GaN nanowires using targets of the respective materials.

Characterization and results

- TEM *(fig. 3.2)*: Core-shell nanowires maintained their length after shell deposition. PLD and WO_3 sulfurization yielded smooth, uniform shells,

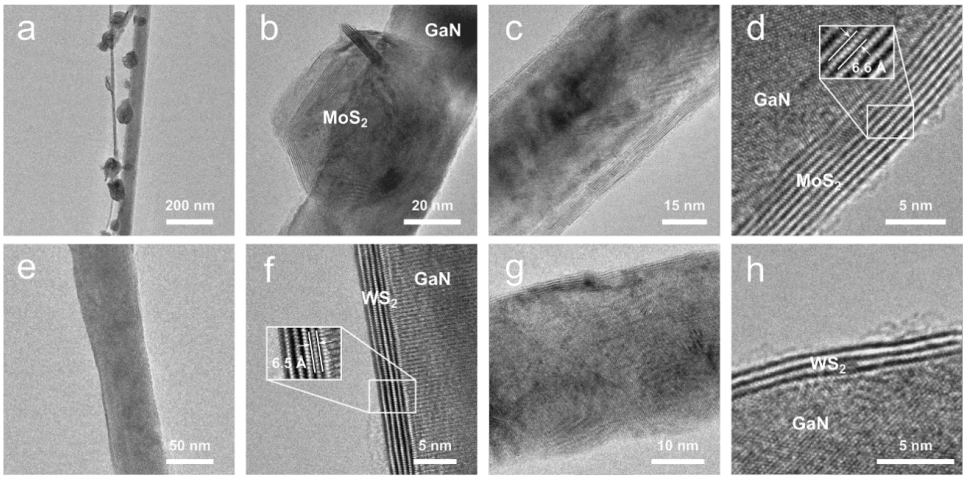

Figure 3.2: Transmission electron microscope images at different magnifications of individual (a-b) GaN-MoS_2 NW prepared via MoO_3 coating sulfurization, (c-d) GaN-MoS_2 NW prepared via pulsed laser deposition, (e-f) GaN-WS_2 NW prepared via WO_3 coating sulfurization, (g-h) GaN-WS_2 NW prepared via pulsed laser deposition; the insets show the measured d-spacings.

while MoO_3 sulfurization resulted in non-uniform island-like coatings. Higher-resolution TEM images revealed the crystalline structure of the MeX_2 shells with parallel atomic planes. Uniform coatings typically ranged from 4 to 10 monolayers, with single-monolayer deposition achievable. Measured interplanar distances for MoS_2 (6.4-6.6 Å) and WS_2 (6.2-6.5 Å) were consistent with bulk values. The GaN core maintained its single-crystalline nature with an interplanar distance of ~3.18 Å.

- XRD Analysis and Raman Spectroscopy *(fig. 3.3)*: X-ray diffraction measurements were conducted to verify the presence of the desired

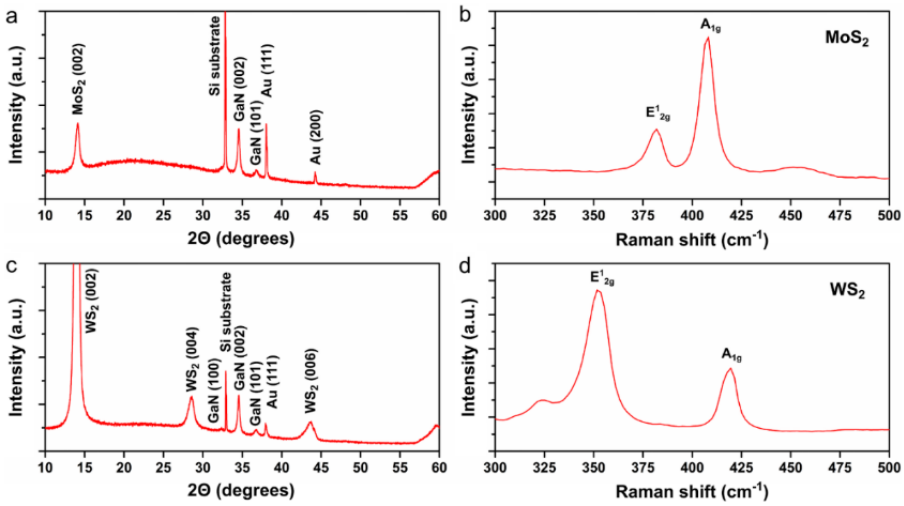

Figure 3.3: (a) X-ray diffraction and (b) micro-Raman spectrum of GaN-MoS_2 NW arrays on a Si/SiO_2 substrate; (c) X-ray diffraction and (d) micro-Raman spectrum of GaN-WS_2 NW arrays on a Si/SiO_2 substrate.

crystalline phases in the core-shell nanowires. The analysis revealed

consistent Bragg peaks corresponding to hexagonal GaN nanowires, MoS_2 shells, and WS_2 shells, aligning with the data obtained from TEM. Additionally, the XRD patterns contained peaks related to the silicon substrate and gold nanoparticles used for vapor-liquid-solid growth, further supporting the accuracy of the characterization and demonstrating the high crystalline quality of the synthesized core-shell nanowires. Room-temperature micro-Raman spectroscopy was employed to provide additional confirmation of the presence of WS_2 and MoS_2 layers in the nanostructures. The spectroscopic results clearly identified the characteristic Raman peaks associated with these TMD materials, further validating the effectiveness of the synthesis process used in this study.

- X-ray photoelectron spectroscopy Analysis *(fig. 3.4)*: it was conducted to confirm the chemical composition of the core-shell nanowires. High-resolution spectra were obtained for Mo 3d, W 4f, S 2p, Ga 3d, and N 1s peaks. For both the GaN-MoS_2 and GaN-WS_2 samples, the S 2p peaks consisted of spin–orbit doublets ($\Delta_{3/2-1/2}$ = 1.2 eV), with the $2p_{3/2}$ peak measured at 161.8 eV, aligning with MoS_2 and WS_2 compounds. In the GaN-MoS_2 nanowires, the Mo 3d peak displayed a spin–orbit splitting

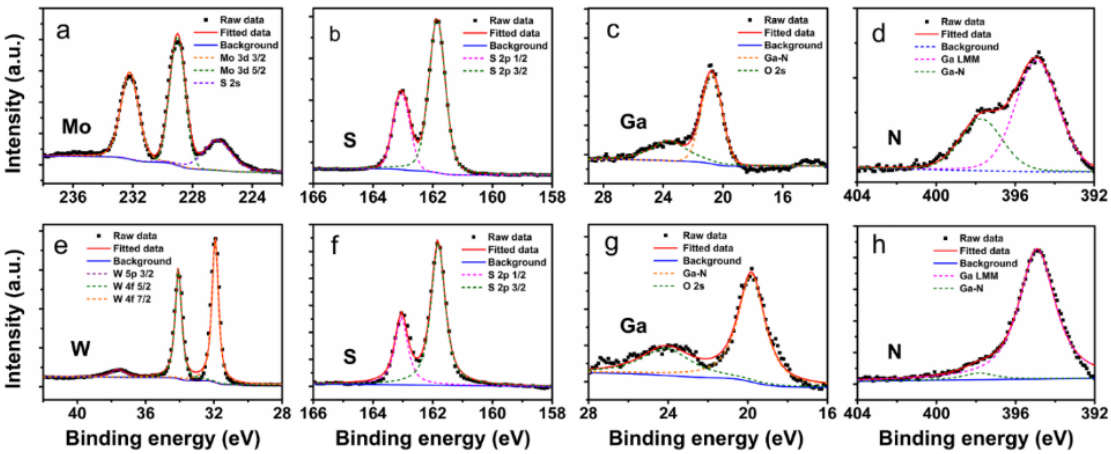

Figure 3.4: High-resolution XPS core-level spectra and peak fits of GaN-MoS_2 core–shell NWs for (a) Mo 3d, (b) S 2p, (c) Ga 3d and (d) N 1 s. High-resolution XPS core-level spectra and peak fits of GaN-WS_2 core–shell NWs for (e) W 4f, (f) S 2p, (g) Ga 3d and (h) N 1s

($\Delta_{5/2-3/2}$ = 3.2 eV), with the Mo $3d_{5/2}$ component at 229.0 eV, consistent with the MoS_2 chemical state. Additionally, the S 2s peak at 226.2 eV was observed in the scan. In the GaN-WS_2 nanowires, the W $4f_{7/2}$ peak for the WS_2 chemical state was measured at 32.0 eV, with a spin–orbit splitting ($\Delta_{7/2-5/2}$ = 2.2 eV).

- Theoretical calculations revealed that, close lattice match between GaN and dichalcogenides, along with favourable atomic arrangement, creates a stable 2D nano heterostructure. The band alignment in these

nanowires is suitable for efficient hydrogen evolution during water splitting under red and near-infrared irradiation. These findings suggest that WS_2-on-GaN and MoS_2-on-GaN core-shell nanowires are promising candidates for photocatalysts in hydrogen production.

Conclusions

This study successfully demonstrated the synthesis of high-quality GaN-MoS_2 and GaN-WS_2 core-shell nanowires using two distinct methods. The characterization results confirmed the formation of well-defined nanostructures with desirable properties. The theoretical analysis further supported the experimental findings, providing insights into the electronic structure of these materials. The synthesized core-shell nanowires hold promise for various applications, including electronics, optoelectronics, and energy-related fields. Future research could explore their potential in areas such as photocatalysis, light-emitting diodes, and field-effect transistors.

3.2 Synthesis of ZnS / Al_2O_3 / $TaSe_2$ - core / shell nanowires

Experimental Method

The ZnS/Al_2O_3/$TaSe_2$ core/shell nanowires were fabricated using a four-step process *(fig. 3.5)*:

I. Growth of ZnS Nanowires: ZnS nanowires were grown on oxidized silicon wafers using a vapor-liquid-solid (VLS) mechanism with gold nanoparticles as catalysts. The ZnS powder was sublimated at 950°C in a quartz tube reactor, and the ZnS vapor was carried to the substrates by an argon/hydrogen gas mixture.
II. Deposition of Al_2O_3 Layer: An Al_2O_3 layer was deposited on the ZnS nanowires using atomic layer deposition (ALD) at 150°C.
III. Magnetron Sputtering of Ta Thin Film: A tantalum (Ta) layer was sputtered onto the ZnS/Al_2O_3 nanowires using DC magnetron sputtering.

IV. Selenization of Ta to $TaSe_2$: The coated nanowires underwent a selenization process through annealing in a selenium-rich environment to convert the Ta layer into $TaSe_2$.

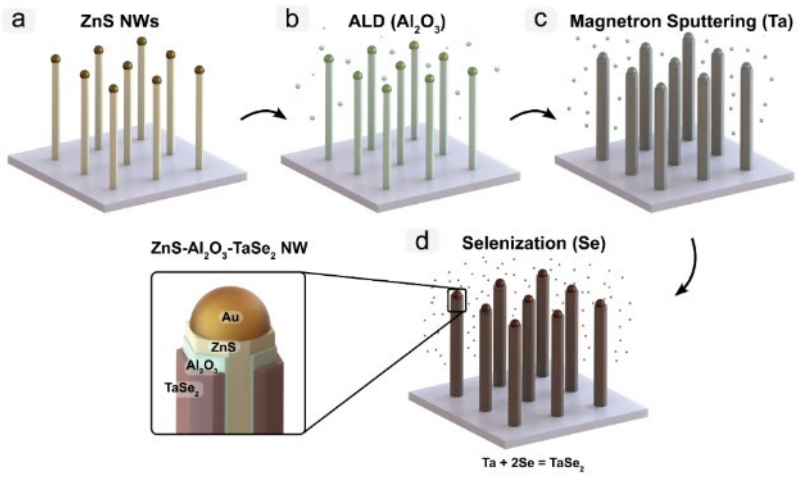

Figure 3.5: A scheme for the four-step method for the fabrication of ZnS/ Al_2O_3/ $TaSe_2$ core/shell NWs. Growth of ZnS NWs via VLS mechanism using Au NPs catalysts (a). Al_2O_3 layer deposition by ALD around ZnS NWs (b). Ta thin film deposition on ZnS/Al_2O_3 NWs (c). Selenization of Ta thin film and formation of NWs ZnS/Al_2O_3/$TaSe_2$ NWs (d)

Characterization and results

- XRD and Rietveld refinement *(fig. 3.6)*: X-ray diffraction (XRD) analysis confirmed the successful selenization of the Ta coating and the presence of the desired phases (ZnS, $TaSe_2$, Al_2O_5). No ZnSe peaks were detected, indicating no selenization of the ZnS core. A β-Ta_2O_5 peak was observed due to potential oxidation of the Ta coating. Additional Bragg peaks were attributed to the substrate and nanoparticles. Rietveld analysis confirmed the phase composition and structural integrity of the ZnS/Al_2O_3/$TaSe_2$ nanowires.
- XPS analysis *(fig. 3.7)*: it was conducted to further validate the chemical states within the shell of the heterostructured nanowires. High-resolution spectra for Ta 4f and Se 3d peaks were acquired, confirming the presence of tantalum selenide in the shell and the absence of additional elements. The Ta 4f scan displayed two doublets, indicating the presence of both $TaSe_2$ (Ta $4f_{7/2}$ peak at 25.2 eV) and Ta_2O_5 (Ta $4f_{7/2}$ peak at 27.0 eV) compounds. The detection of Ta_2O_5 is likely due to the oxidation of the Ta coating during

handling or storage. The Se $3d_{5/2}$ peak at 55.6 eV with a spin-orbit splitting of 0.86 eV confirmed the presence of tantalum selenide in the core-shell nanowires. Overall, the XPS analysis provides strong evidence for the successful formation of the $TaSe_2$ shell and highlights the importance of careful handling and storage to prevent oxidation and maintain the stability of the heterostructures.

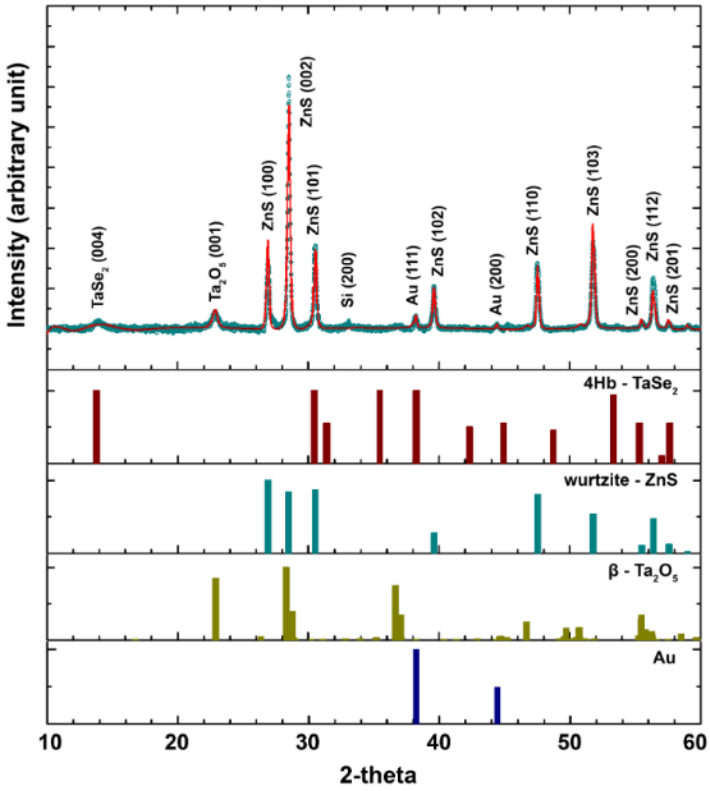

Figure 3.6: Rietveld refinement (solid line) of the X-ray diffraction pattern (open circles) for selenized $ZnS/Al_2O_3/Ta$ NWs on an oxidized Si/SiO_2 substrate. The corresponding Bragg indexes for each crystalline phase have been identified and marked, as well as XRD patterns for 4Hb-$TaSe_2$, wurtzite ZnS phase, β-Ta_2O_5 and Au.

- TEM analysis *(fig. 3.8)*: it was used to examine the morphology and internal structure of the core/shell nanowires. The TEM images revealed gold nanoparticles at the ends of the nanowires, confirming the use of the vapor-liquid-solid growth mechanism. A layer of $TaSe_2$ was observed surrounding the nanowires, with a thickness ranging

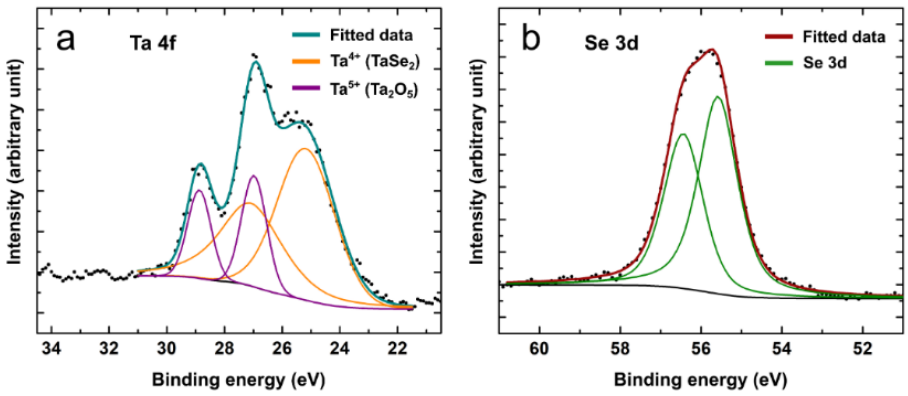

Figure 3.7: High-resolution XPS spectra of the selenized $ZnS/Al_2O_3/Ta$ NWs elements for (a) Ta and (b) Se. Ta 4f peak scan fitting revealed two chemical states (Ta 4+ and 5+) present in the sample.

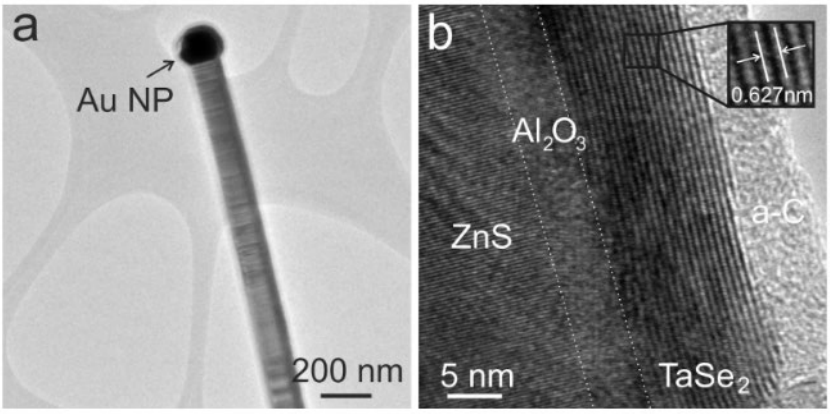

Figure 3.8: TEM images of ZnS/Al_2O_3/$TaSe_2$ NWs at different magnifications. A single ZnS/Al_2O_3/$TaSe_2$ NW with a Au NP at the end on a Lacey carbon-coated TEM grid (a). ZnS/Al_2O_3/$TaSe_2$ NW at high magnification; the individual layers of the heterostructure are identified, and amorphous carbon (a-C) is also present on top of the $TaSe_2$ shell (b).

from 10 to 20 layers and an interlayer distance of approximately 0.627 nm. A non-crystalline carbon layer was found on top of the $TaSe_2$ surface. While atomic resolution of the Al_2O_3 interlayer was not achieved, the observed amorphous spacing thickness aligned with the expected thickness. In an additional experiment with ZnO/Al_2O_3/Ta nanowires, the ZnO core sublimated during selenization, but the Al_2O_3 shell remained intact, demonstrating the stability of the Al_2O_3 barrier.

Conclusions

This study successfully fabricated ZnS/Al_2O_3/$TaSe_2$ core/shell nanowires using a four-step process involving vapor-liquid-solid growth, atomic layer deposition, magnetron sputtering, and selenization. Comprehensive characterization techniques confirmed the formation of the desired core/shell structure with well-defined layers. The ZnS core remained intact throughout the selenization process, while the Ta layer was successfully transformed into a $TaSe_2$ shell. The Al_2O_3 interlayer acted as a protective barrier, preventing the ZnS core from reacting with the selenium. This work introduces a scalable - versatile method for fabricating core/shell nanowires with 2D TMD shells. The technique can be applied to various chalcogenides and metal precursors, expanding the potential for creating diverse set of nanostructures.

3.3 Unique aspects of this chapter

GaN-MoS_2 and GaN-WS_2 Heterostructures: While previous research [66–69] has explored planar heterostructures of these materials, our approach offers a

novel core-shell nanowire configuration. This increased surface area could enhance their catalytic activity, particularly for HER applications. We compared two synthesis methods: direct PLD deposition and a combination of magnetron sputtering and CVT.

ZnS-Al_2O_3-$TaSe_2$ Heterostructures: $TaSe_2$, typically studied in exfoliated form [70,71], is here synthesized as a shell on a ZnS nanowire core. This approach increases surface area and enables scalable production. By avoiding thermally stable Ta_2O_5 as a precursor, we simplified the synthesis process. The use of ZnS and Al_2O_3 layers demonstrates the potential for creating complex heterostructures of varied chalcogen groups together with tailored properties.

4. Growth of TMDs thin films

4.1 WSe_2 thin films and crystals

Experimental Method

The synthesis of WSe_2 thin films was conducted using the chemical vapor transport (CVT) method *(fig. 4.1)*. This technique involves the sublimation of a precursor material (WO_3 or W metal) in a sealed ampoule containing a transport agent (selenium). The precursor reacts with selenium to form WSe_2, which is then transported to a cooler region where it condenses as a thin film on a substrate.

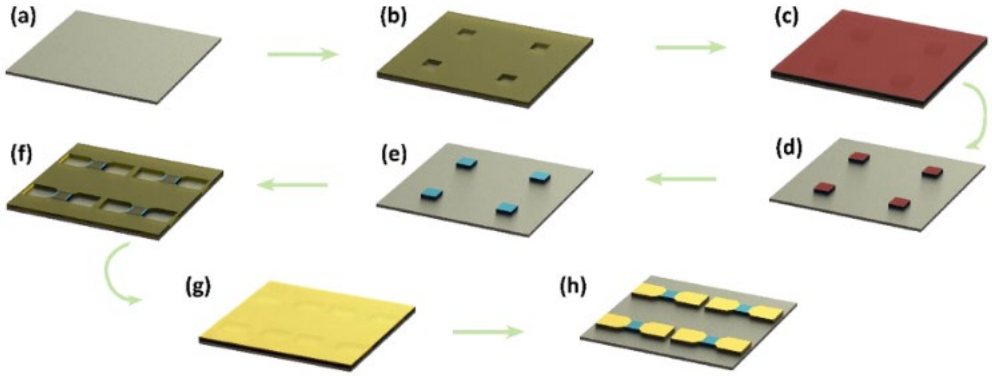

Figure 4.1: Schematic of the process of on-chip device fabrication. First the SiO_2/Si substrate is cleaned using acetone and isopropanol (a), then the first mask is made using the standard photolithography process (b) on which precursor material is deposited (c). After first mask lift-off, the precursor material film is in the desired pattern (d) which is subsequently selenized (e). Afterwards, the second photoresist mask is deposited (f) for the deposition of contact material (Cr ~ 5 nm, Ag ~ 95nm, Al ~ 50 nm) using the thermal evaporation method (g) followed by lift-off to obtain the photoconductor device array on a chip (h).

Results and discussion

- Scanning Electron Microscopy *(fig. 4.2)*: SEM analysis revealed that films from WO_3 typically had larger crystals, reaching up to 1 µm at higher temperatures (800 °C), while films from the W metal precursor had smaller, more consistent crystals with clear boundaries, with diameters of 0.5 µm regardless of temperature.
- Atomic Force Microscopy *(fig. 4.3)*: AFM Z-drive images further supported these observations, with films from WO_3 showing more random crystal growth, while those from W metal had flatter surfaces with more uniform

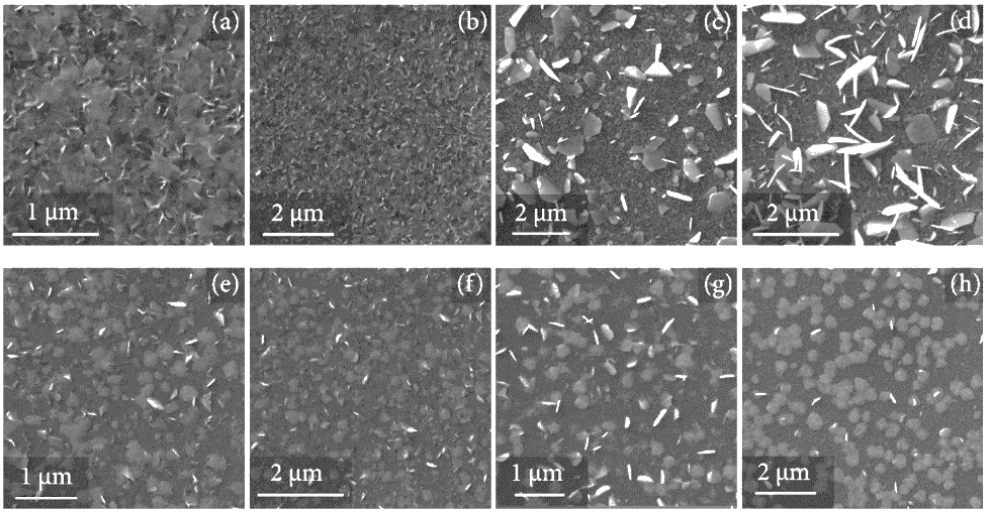

Figure 4.2: Scanning electron microscope images at different magnifications of WSe_2 films made from a WO_3 precursor at 700°C (a,b) and 800°C (c,d) and from a W metal precursor at 700°C (e,f) and 800°C (g,h)

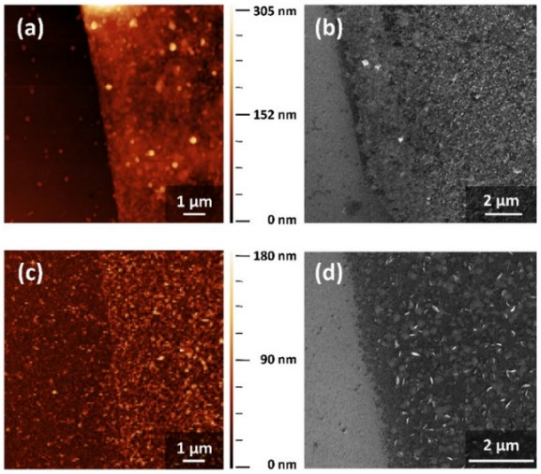

Figure 4.3: Atomic force microscope (AFM) Z-drive images of WSe_2 films made from a WO_3 precursor (a) and from a W metal precursor (c) showing the difference between film surfaces and further complimented by SEM images of the same samples in the respective order of (b) and (d)

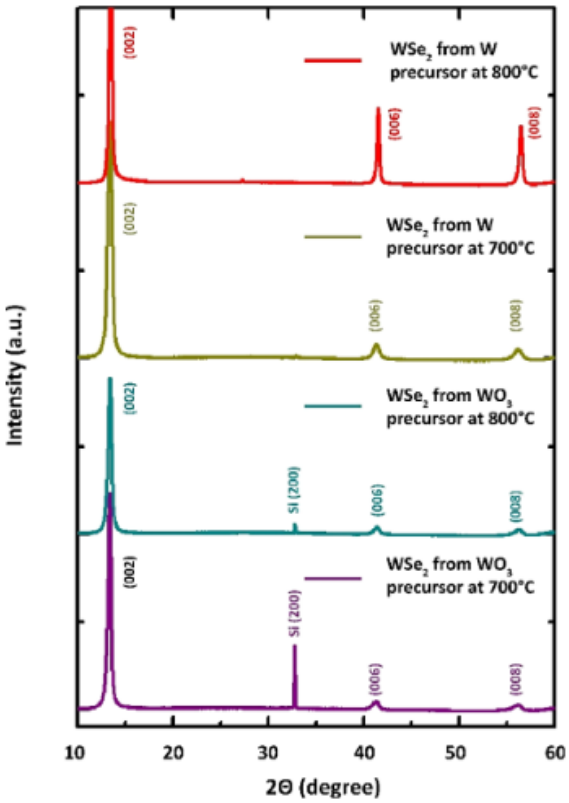

Figure 4.4: X-ray diffraction patterns of WSe_2 films from both precursors (WO_3 and W) at different temperatures, 700°C and 800°C, show peaks confirming the phase of the synthesized WSe_2 film

crystal distribution. The out-of-plane crystal growth in WO3-based films could be due to vapor-phase selenization and re-deposition of WSe_2.

- X-ray Diffraction *(fig. 4.4)*: XRD patterns obtained from films synthesized from both WO_3 and W metal precursors exhibited characteristic peaks corresponding to crystalline WSe_2, indicating the successful formation of the desired phase. No extraneous peaks attributable to secondary phases or impurities were detected.
- Micro-Raman Spectroscopy *(fig. 4.5)*: The presence of distinct Raman peaks centred around 250.2 cm^{-1} and 259 cm^{-1} unequivocally confirmed the formation of WSe_2, corresponding to the in-plane (E12g) and out-of-plane (A1g) vibrational modes, respectively.

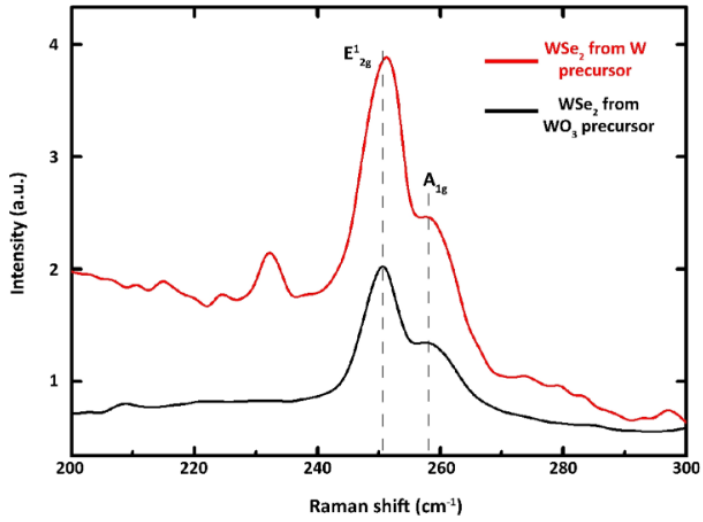

Figure 4.5: Raman spectra of WSe_2 thin films synthesized from both precursors (WO_3 and W) using CVT method showing the peaks respective to E^1_{2g} and A^1_g vibrational modes

- Electrical Characterization: WSe_2 films synthesized from WO_3 precursors exhibited superior photoelectric performance compared to those from W metal precursors. The output and transfer curves for FETs made from WO_3-based films displayed stronger field-effect and p-type conductivity, suggesting better electrical properties.

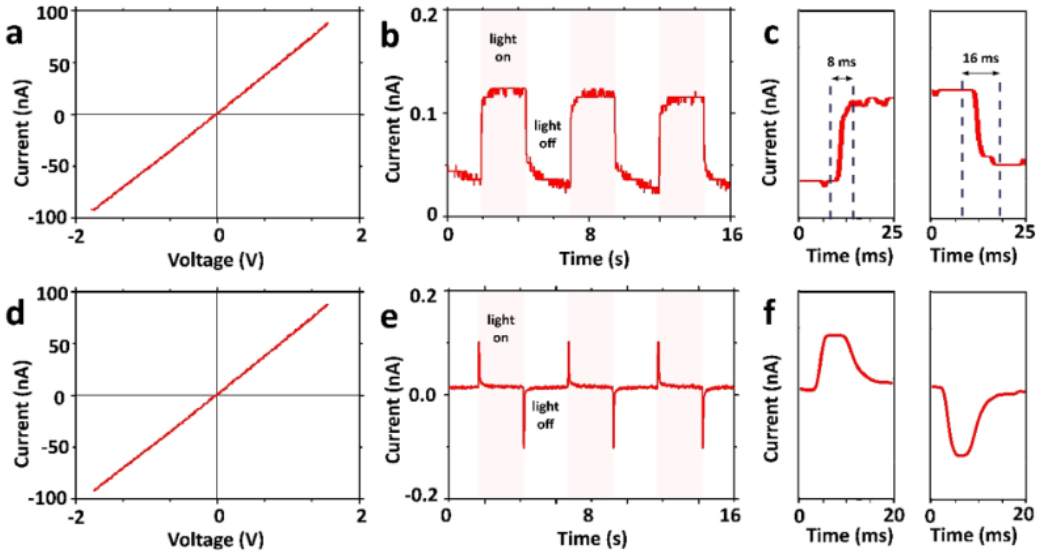

Figure 4.6: WSe_2 two-terminal photoconductor devices prepared from WO_3 and W metal as the precursor materials, respectively, showing dark state I–V characteristics (a,d), on–off response (b,e), and response time (c,f) measurements at 2 V bias voltage and 1 W/cm² light intensity with a 405 nm wavelength light source.

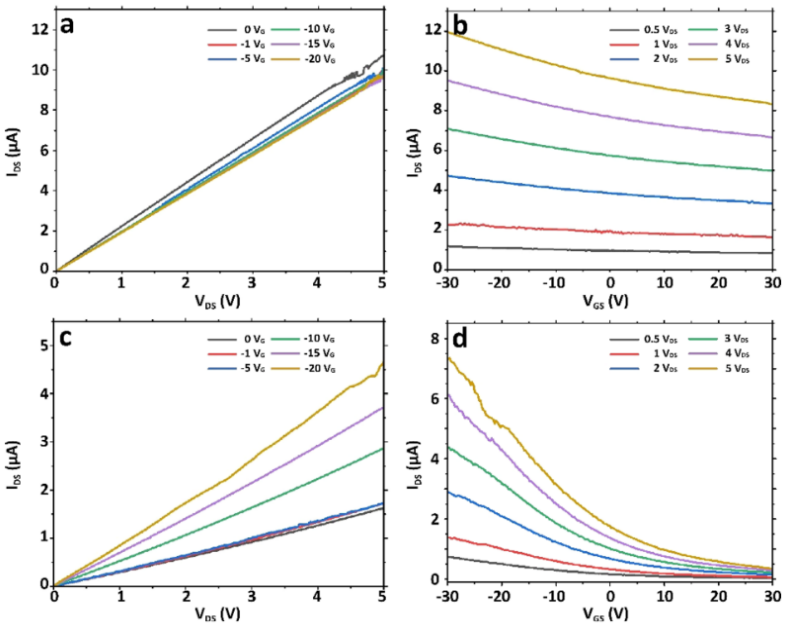

Figure 4.7: WSe_2 two-terminal photoconductor devices, prepared from W(a,b) and WO_3(c,d) metal as the precursor (I_{DS}-drain source current, V_{DS}-drain source bias voltage, V_{GS}- gate source bias voltage).

Conclusion

WSe_2 films grown from W metal precursors exhibited smaller, more uniform crystal sizes, WO_3-based films demonstrated superior photoelectric performance, despite their larger and more randomly oriented crystals. This suggests that factors beyond crystal morphology, such as interfacial interactions or impurity incorporation, play a crucial role in determining the photoelectric properties of WSe_2 films synthesized using the CVT method. Both WO_3 and W-based films exhibited p-type conductivity, indicating their potential for electronic applications. However, the superior photoelectric performance of WO_3-based films highlights the importance of precursor selection in optimizing the properties of WSe_2 thin films for optoelectronic devices.

4.2 $ReSe_2$ thin films

Experimental Method

The study investigated the synthesis of $ReSe_2$ thin films using chemical vapor transport. Rhenium (Re) and rhenium oxide (ReO_x) films were deposited mainly on sapphire (c-plane) substrates using magnetron sputtering *(fig. 4.8)*. To optimize the synthesis temperature, temperatures ranging from 550°C to 1000°C were explored for both Re metal and ReO_x precursors. Initial XRD patterns were obtained to analyse the reaction progress and product formation. Temperature optimization was done based on the initial XRD analysis, the temperature range was narrowed down to 650°C to 850°C for the optimal synthesis of $ReSe_2$ thin films. Lower temperatures resulted in incomplete reactions (leftover precursor), while higher temperatures led to the reduction

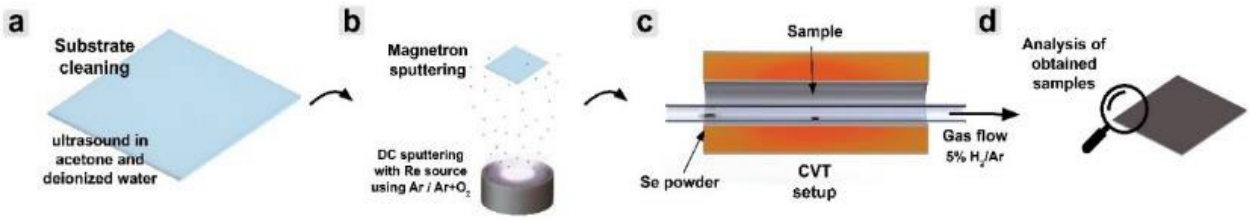

Figure 4.8: Graphical illustration of the methodology followed in this work starting with (a) substrate preparation by cutting them in ~100 mm² square size and cleaning them in ultrasound, (b) magnetron sputtering of Re and ReO_x precursor films, (c) selenization process at elevated temperatures in horizontal quartz tube CVT setup for 15 minutes followed by (d) analysis of the synthesized material via various techniques.

of $ReSe_2$ films to Re metal. The presence of H_2 in the carrier gas accelerated the reaction and selenization rate.

Characterization and results

- XRD analysis *(fig. 4.9)*: It conducted to characterize the synthesized $ReSe_2$ thin films. The obtained XRD patterns were compared with the reference data (ICDD card no. 04-007-1113) and previous studies on this material. The analysis revealed the formation of highly crystalline $ReSe_2$ films with a distorted 1T' structure, which has triclinic symmetry ($P\bar{1}$). This crystal structure was confirmed to be stable within the temperature range of 650°C to 850°C. The presence of the characteristic peaks in the XRD patterns,

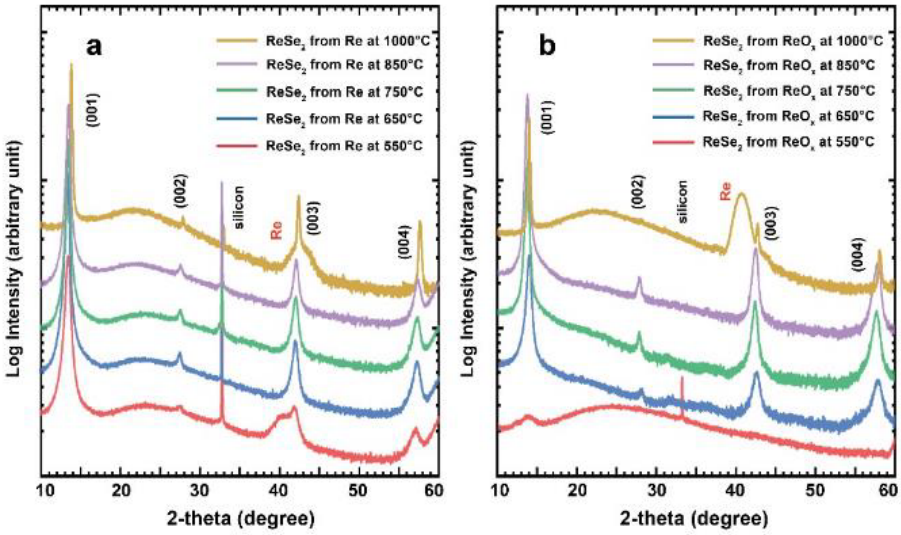

Figure 4.9: X-ray diffraction patterns for the synthesized $ReSe_2$ films from (a) Re metal precursor films and (b) ReO_x precursor films at 650°C, 750°C, 850°C and 1000°C on SiO_2/Si substrate for 15 minutes.

matching those reported in previous studies, strongly supports the successful synthesis of $ReSe_2$.

- SEM and AFM analysis *(fig. 4.10 and 4.11)*: SEM analysis revealed a noticeable increase in surface roughness for both Re and ReO_x precursor-

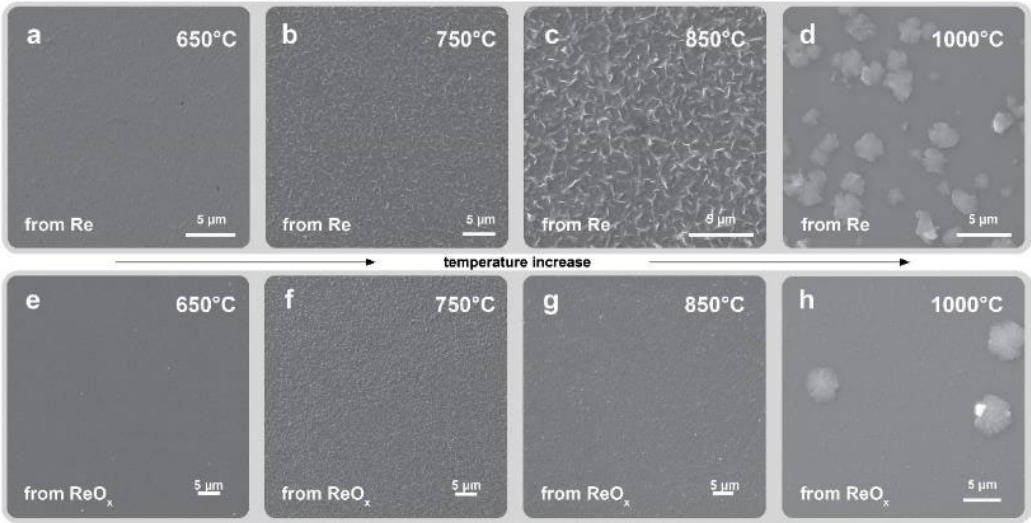

Figure 4.10: SEM images of the synthesized $ReSe_2$ films from (a-d) Re metal precursor films and (e-h) ReO_x precursor films using 650°C to 1000°C temperatures on silicon as substrate.

based films with increasing synthesis temperature. Re-derived films exhibited pronounced out-of-plane filamentary structures at higher temperatures, likely due to the expansion of Re metal during selenization. AFM results showed a highly conductive, fine-grained surface with

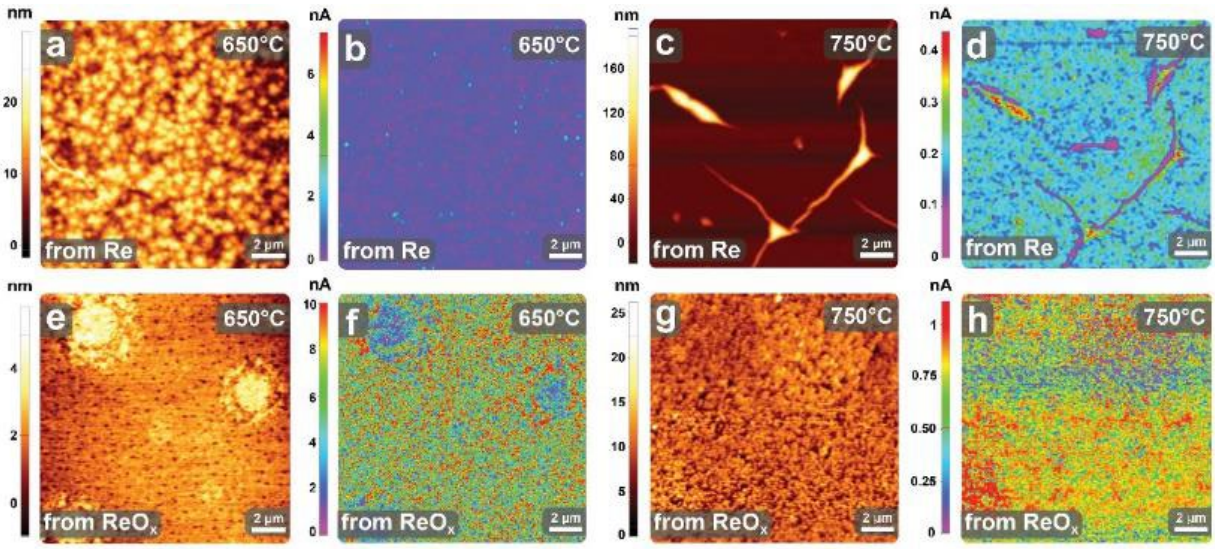

Figure 4.11: AFM images of the synthesized $ReSe_2$ films on sapphire substrate from (a-d) Re metal precursor and (e-h) ReO_x precursor at 650°C and 750°C temperatures are shown here. Fig. a, c, e, g are topographical images and fig. b, d, f, h are of conductive AFM measurements with platinum tip and 0.02V bias. All images were taken in 255 µm² area.

crystallite sizes ranging from 50 to 100 nm. Re-derived films synthesized at 650°C exhibited significant roughness, while ReOx-derived films had a smoother texture. At 750°C, Re-derived films displayed pronounced out-of-plane filamentary structures, indicating substantial changes in surface morphology. Conductivity mapping revealed variations in conductivity distribution for both types of films. Re-derived films at 650°C showed varied conductivity due to rough surface morphology, while ReOx-derived films had a more homogeneous conductivity distribution. At 750°C, Re-derived films continued to show significant conductivity variations, while ReOx-

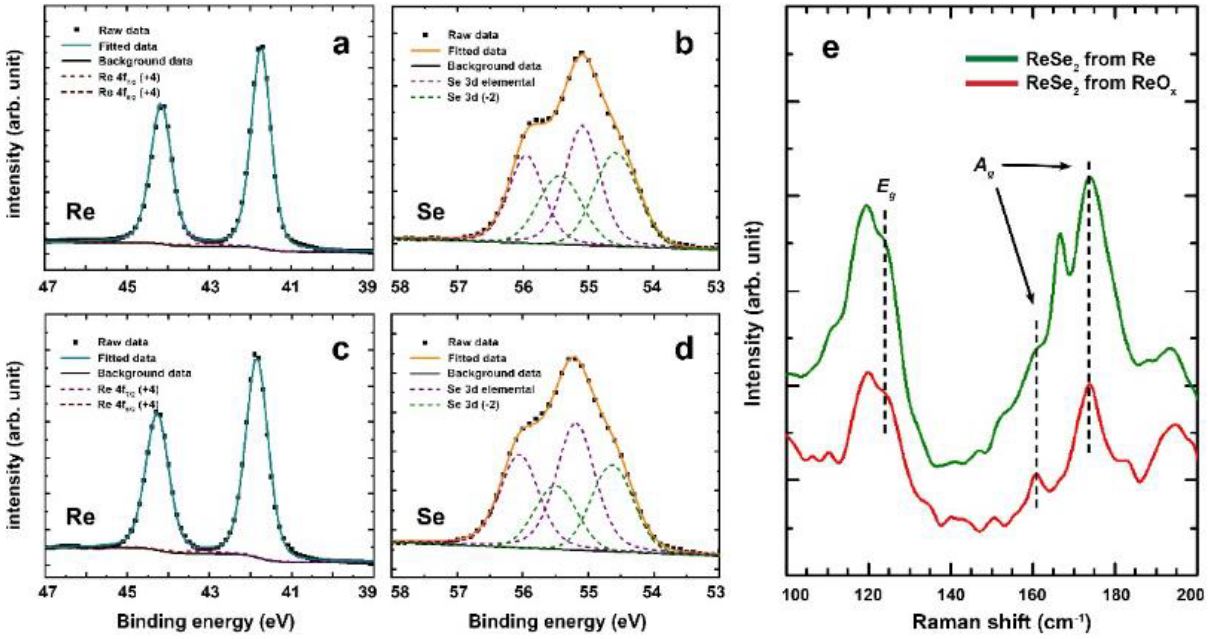

Figure 4.12: XPS spectra of $ReSe_2$ films synthesized at 650°C from (a,b) Re precursor films and (c,d) ReO_x precursor films. (e) Raman spectra of the $ReSe_2$ films synthesized at 650°C measured with 532 nm wavelength laser.

derived films maintained a more uniform conductivity distribution.

- XPS and Raman analysis *(fig. 4.12)*: XPS analysis was conducted to determine the chemical states of elements in the $ReSe_2$ films. The XPS spectra revealed the presence of only Re and Se elements, along with organic surface contaminants. The Re 4f peak displayed a single doublet with a spin-orbit splitting of 2.43 eV and an area ratio of 4:3. The Re $4f_{7/2}$ peak was located at approximately 41.8 eV, indicating a valence state of 4+ in the $ReSe_2$ compound. The Se 3d peak displayed two doublets with a spin-orbit splitting of 0.86 eV. The first doublet at 54.7 eV corresponded to the 2- chemical state in $ReSe_2$, while the second doublet at 55.2 eV suggested the presence of elemental Se on the selenide surface. Raman spectroscopy further verified the composition and structure of the $ReSe_2$ films. The Raman spectra revealed distinct vibrational modes corresponding to the E_g and A_g modes of $ReSe_2$, aligning well with previous studies. These modes are characteristic of the in-plane and out-of-plane vibrations of Re and Se

atoms in the $ReSe_2$ crystal lattice. The consistency of these Raman peaks with literature values confirms the successful formation of $ReSe_2$ with the expected crystalline structure and chemical composition.

- Optical and Nonlinear measurements *(fig. 4.13, 4.14 and 4.15)*: Reflectance

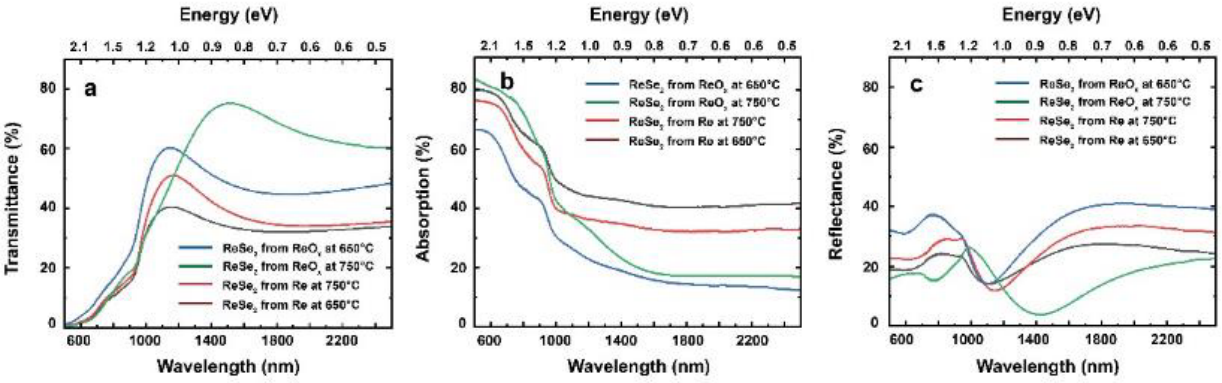

Figure 4.13: (a) Transmittance, (b) absorption and (c) reflectance of the produced $ReSe_2$ films on sapphire substrate from both precursor materials in the range of 500-2500 nm wavelength.

measurements revealed that $ReSe_2$ films synthesized from ReO_x at 650°C exhibited higher reflectance at wavelengths >1200 nm compared to those synthesized at 750°C. All synthesized films exhibited a dark grey colour and high absorption (70-80%) in the visible light range, due to their small direct optical band gap of approximately 1.2 eV. The electrical properties of the samples could not be determined due to inconsistent Hall voltages. This

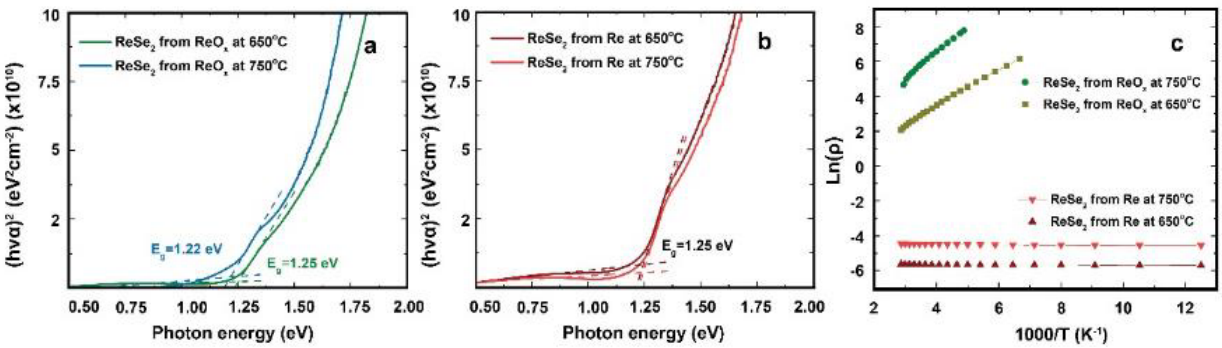

Figure 4.14: Tauc plot to deduce the direct optical bandgap of the $ReSe_2$ films synthesized from (a) ReO_x and (b) Re metal. (c) Change in Resistivity with temperature was measured using Van der Pauw configuration with a Hall effect system. Used samples for these measurements were covered with $ReSe_2$ films in 100 mm^2 square area.

inconsistency was likely caused by either very low carrier mobility (<1 cm^2/Vs) or very high carrier concentration (>10^{21} cm^{-3}), both of which were outside the measurable range of the system. In contrast, samples

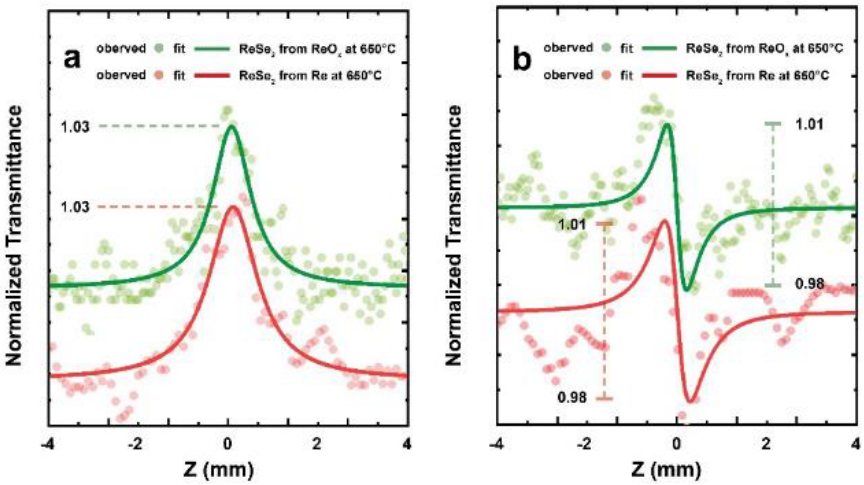

Figure 4.15: Open aperture Z-scan curves of the $ReSe_2$ thin films (a) synthesized from Re at 650°C and 750°C measured with the power of 16.4 W and 20.1 W respectively, (b) from ReO_x at 650°C and 750°C with the power of 21.2 W and 24.2 W with 900nm wavelength laser source.

derived from Re exhibited higher conductivity and metallic behaviour. The activation energy (Ea) derived from the data for the semiconducting films derived from ReOx was 92 meV at 650°C and 131 meV at 750°C.

The Z-scan method was used to assess the nonlinear optical properties of the $ReSe_2$ films. A Kerr signal was consistently observed for all samples, with a value of $n_2 = (-1.23 \pm 0.65) \times 10^{-2}$ cm^2/W. The saturation absorption coefficient (β) was measured to be -950 ± 290 cm/GW for Re-derived films and -730 ± 330 cm/GW for ReO_x-derived films. These findings suggest that $ReSe_2$ films have potential applications in ultrafast laser systems due to their nonlinear optical properties. The saturation absorption coefficient and Kerr nonlinearity values indicate that these films could be suitable for Q-switching or mode-locking in laser systems.

Conclusion

This study successfully synthesized $ReSe_2$ thin films from both Re metal and ReO_x precursors using magnetron sputtering and atmospheric pressure CVT. Characterization techniques confirmed the formation of $ReSe_2$ in both cases. The optimal synthesis temperature range for $ReSe_2$ thin films was found to be between 650°C and 750°C. Re-derived films exhibited out-of-plane elongated structures at higher temperatures, while ReOx-derived films remained relatively smooth. Optical properties were largely unaffected by the synthesis temperature, although Re metal films were less sensitive to changes. The $ReSe_2$ films showed potential for applications in nonlinear optics, such as Q-switching and mode-locking in laser systems. Semiconductor behaviour was observed only in films derived from ReO_x, highlighting the impact of precursor choice on electronic properties.

$ReSe_2$ thin films, synthesized in this study, show promise for applications in nonlinear optics and electrocatalysis. Their semiconductor behaviour and unique combination of electrical and optical properties make them potential candidates for various electronic devices. This study contributes to the understanding of TMD materials and their synthesis. Future research can explore the effects of different synthesis parameters and the integration of $ReSe_2$ into specific applications.

4.3 $TiSe_2$ and VSe_2 thin films

Experimental Method

The synthesis of $TiSe_2$ and VSe_2 involved a two-step process *(fig. 4.16)*:

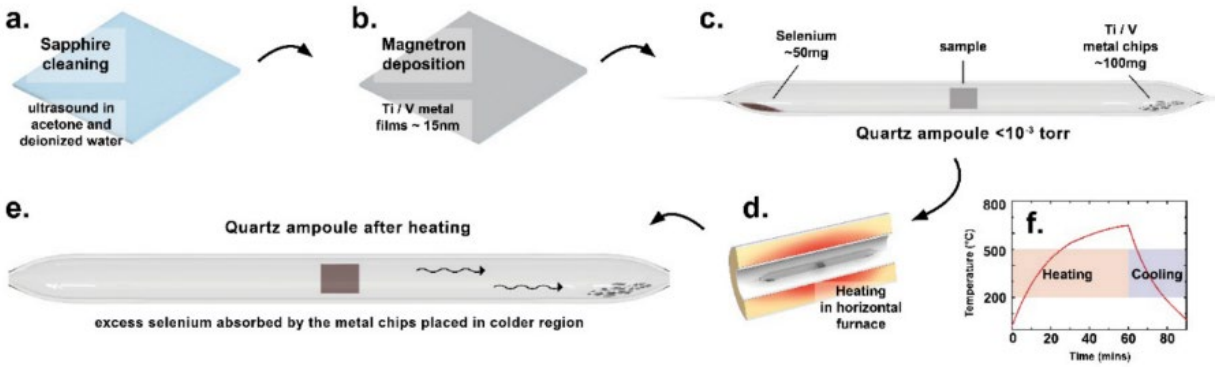

Figure 4.16: Graphical illustration of the methodology used here to synthesize $TiSe_2$ and VSe_2 thin films starting from (a) substrate cleaning in acetone and DIW using ultrasound for 5 mins each, followed by (b) deposition of Ti / V metal film using magnetron sputtering (c) sample placed in a quartz ampoule with Se powder and respective metal chips in shown configuration (d) ampoules heated up using a horizontal furnace (e) after heating the ampoule, no excess selenium vapour were found near edges of any ampoules. (f) heating cycle of an ampoule, shown with ramp rate of heating and cooling.

I. Magnetron sputtering: Thin metal precursor films (Ti or V) were deposited on substrates using magnetron sputtering.
II. Selenization: The deposited films were annealed in a selenium-rich environment to convert them into the corresponding diselenide.

Key Parameters:

- Precursor thickness: 15 nm was found to be optimal for continuous diselenide films.
- Selenium environment: A sealed vacuumed quartz ampoule with excess selenium was used to ensure complete selenization.
- Temperature: The optimal synthesis temperature was determined to be between 700°C and 750°C for both $TiSe_2$ and VSe_2.

From the experiments, a 15 nm thickness of the metal precursor resulted in continuous diselenide films after the selenization process, so that thickness value was kept constant for all samples of this study. Initially, when ampoules were made without their respective metal chips (Ti/V), excess selenium vapor condensed near the edges of the samples or formed droplets on top of the synthesized material. To resolve this, extra metal chips were introduced after several trials, which eliminated the excess Se issues and yielded the best results. It's noteworthy that attempts to selenize Ti/V films using elemental Se in a quartz tube at atmospheric pressure did not trigger the desired chemical reaction.

Characterization and Results

- XRD and SEM Analysis *(fig. 4.17 and 4.18)*: XRD patterns confirmed the

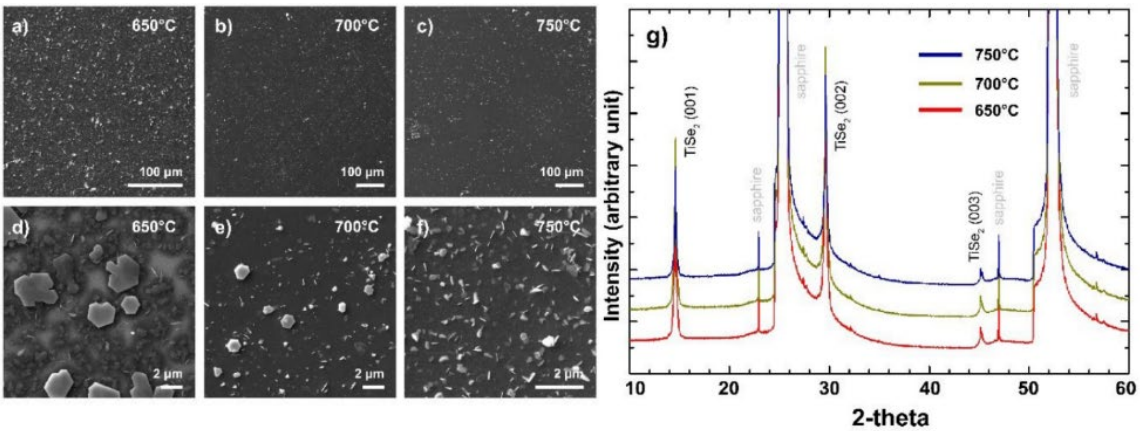

Figure 4.17: SEM images of $TiSe_2$ thin films (a,d) converted at 650°C, (b,e) at 700°C and (c,f) at 750°C. (g) XRD spectra of $TiSe_2$ thin films synthesized using different temperatures.

successful synthesis of crystalline $TiSe_2$ and VSe_2 for all temperatures. $TiSe_2$ films synthesized at 650°C had a rougher surface with larger crystals, while films synthesized at higher temperatures were smoother. VSe_2 films

synthesized at 650°C exhibited out-of-plane nanocrystals, making them rougher compared to films synthesized at higher temperatures.

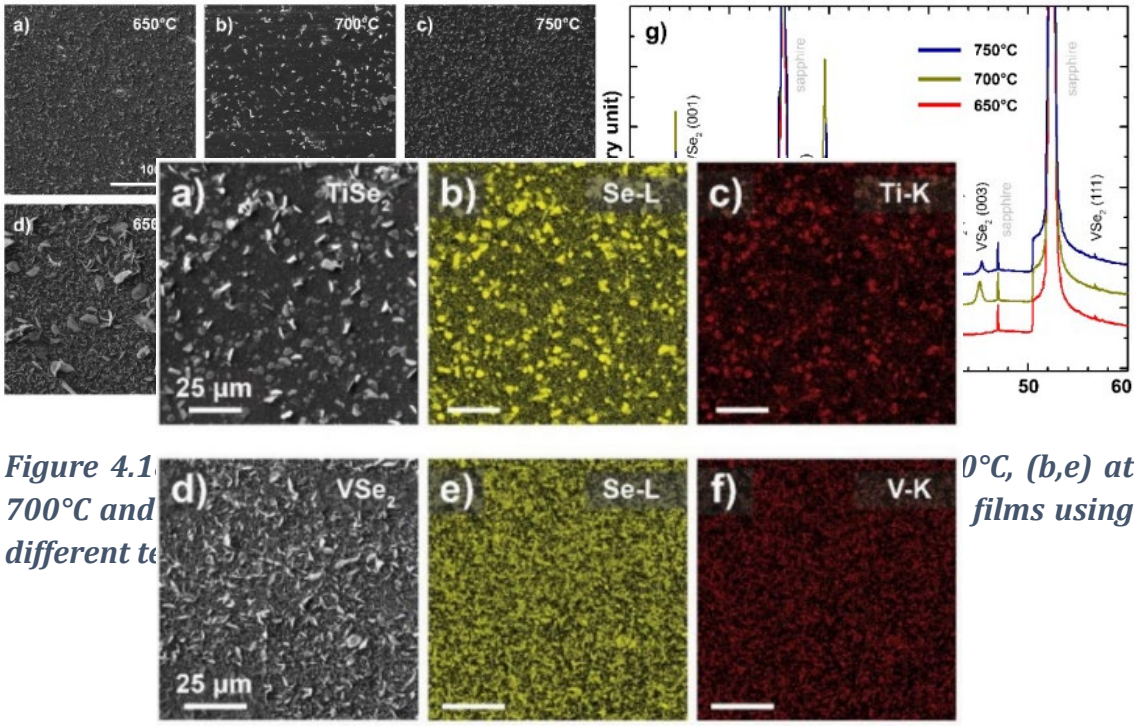

Figure 4.1 0°C, (b,e) at 700°C and films using different te

Figure 4.19: EDX elemental mapping of (a-c) $TiSe_2$ and (d-f) VSe_2 films synthesized at 650°C, shows presence and distribution of their respective elements across the film.

- EDX Analysis *(fig. 4.19)*: Chemical composition: EDX measurements confirmed the proper stoichiometry of Ti/V and Se (1:2) in the synthesized films.

Conclusions:

This study explored the large-scale synthesis of $TiSe_2$ and VSe_2 thin films using a two-step process, with characterization performed via SEM, EDX, XRD, and XPS to assess their quality and composition. Both $TiSe_2$ and VSe_2 films displayed hexagonal surface crystals, varying in size and number depending on synthesis temperature. Despite temperature changes, the films remained continuous post-selenization. XRD and XPS confirmed the presence of $TiSe_2$ and VSe_2. The optimal synthesis temperatures were found to be 650-750°C for $TiSe_2$ and 700-750°C for VSe_2. EDX analysis revealed higher concentrations in surface crystals compared to the rest of the film, further confirming film continuity. This

approach offers a scalable method for producing continuous $TiSe_2$ and VSe_2 films on various substrates. It also presents potential for extending to other TMD materials, which could benefit applications in electronics, energy storage, and catalysis.

4.4 Unique aspects of this chapter

WSe_2: While prior research often relies on exfoliation or CVD techniques for WSe_2 synthesis [72–74], our approach focuses on a scalable method involving standard photolithography for geometry control. The synthesized WSe_2 exhibited p-type conductivity, demonstrating its potential for electronic applications, although not achieving the pristine quality of exfoliated or MBE-grown materials.

$ReSe_2$: Similar to WSe_2, $ReSe_2$ is typically synthesized through exfoliation or CVD techniques [75–77]. Our method offers a scalable approach, yielding high-quality films with non-linear optical properties. Additionally, using Re metal as a precursor resulted in a unique surface texture, promising applications in surface-sensitive areas like photocatalysis.

$TiSe_2$ and VSe_2: The synthesis of $TiSe_2$ and VSe_2 required a modified approach due to the high thermal stability or instability of their metal precursors [78,79]. A quartz ampoule technique was employed to create local low pressure and high selenium vapor pressure, enabling the conversion of metal precursors into their respective diselenide. This method offers a potential pathway for large-scale production of these materials, which is often overlooked in conventional approaches.

5. Summary: Objectives in retrospect

1. The study developed innovative synthesis techniques tailored for producing thin films of transition metal dichalcogenides on diverse surface morphologies, spanning from one-dimensional nanowires to two-dimensional silicon and sapphire wafers. It explored a wide array of TMD materials, achieving successful growth of GaN/MoS_2 and GaN/WS_2 core–shell nanowires, ZnS/Al_2O_3/$TaSe_2$ nanowires, and WSe_2 on silicon, as well as $ReSe_2$, $TiSe_2$, and VSe_2 on sapphire substrates.

2. The study introduced novel synthesis techniques for transition metal dichalcogenides utilizing the respective transition metal as a precursor, bypassing the use of their thermally stable oxides. Specifically, $TaSe_2$ and $TiSe_2$ were synthesized from Ta and Ti metal, respectively, employing a two-step process. Initially, metal deposition was accomplished using DC magnetron sputtering, followed by the selenization of the precursor film within a vacuum-sealed quartz ampoule.

3. In this study, WSe_2 and $ReSe_2$ were successfully synthesized from their respective metal and oxide precursors using a two-step synthesis approach. Magnetron sputtering was employed to deposit the precursors onto the substrate, followed by selenization under atmospheric pressure using chemical vapor transport. This methodology, involving two types of precursors to achieve the same TMD material, facilitated a comparative analysis of the electrical properties and morphological differences between the synthesized TMDs. This comparison highlighted potential advantages of using specific precursors for particular applications.

4. The chemical and structural properties of the produced materials, MoS_2, WS_2, WSe_2, $ReSe_2$, $TaSe_2$, $TiSe_2$, and VSe_2, were comprehensively investigated using a range of characterization techniques. X-ray diffraction, Raman spectroscopy, and X-ray photoelectron spectroscopy were employed to analyse the crystalline structure and chemical composition of the synthesized materials. Additionally, scanning electron microscopy, transmission electron microscopy, and atomic force microscopy were utilized for detailed imaging and morphological analysis. These characterization methods provided a deeper understanding of the properties of each material, allowing for exploration of their potential applications in various fields. The obtained data will serve as a valuable resource for future investigations in this field,

facilitating further research and development in the study of transition metal dichalcogenides.

5. In this study, standard photolithography techniques were employed to precisely control the geometry of the produced WSe_2 thin films, enabling the fabrication of tailored devices to meet specific application requirements. By integrating photolithography into the synthesis process, we successfully demonstrated the fabrication of two-contact field-effect transistors (FETs) using the synthesized WSe_2 material. Through systematic measurements and analysis conducted on the FETs, we gained insights into the electrical behaviour and performance of the synthesized material, paving the way for potential applications in electronic and optoelectronic field.

6. Main theses

1. Using Pulsed Laser Deposition, well-layered MoS_2 and WS_2 shells can be produced around GaN nanowires at temperatures near 650°C and a process pressure of $\sim 10^{-5}$ torr. Known for their potential in hydrogen evolution applications, GaN/MoS_2 and GaN/WS_2 in this core-shell nanowire form exhibit significantly increased reactive surface area, thereby enhancing their applicability in hydrogen evolution reactions. [A1]

2. Layered $TaSe_2$ is possible to produce on a variety of morphological substrates (1D nanowires, 2D flat wafers) by selenizing magnetron sputtered Ta metal film around 650°C in a vacuum-sealed quartz ampoule ($\sim 10^{-3}$ torr base pressure). [A2]

3. Patterned p-type WSe_2 thin films can be produced by integrating standard photolithography with the process of selenizing magnetron-sputtered WO_3 in a chemical vapor transport system at temperatures around 750°C and ambient pressure. [A3]

4. $ReSe_2$ film formation, achieved by selenization of magnetron-sputtered Re and ReO_x films in 750°C-850°C range using an ambient pressure chemical vapor transport system, results in films of distinct surface morphology depending on the precursor used. $ReSe_2$ films derived from Re metal exhibit a more textured surface, whereas those derived from ReO_x produce a smoother surface. [A4]

5. Production of $TiSe_2$ and VSe_2 thin films is achievable from their respective magnetron-sputtered metal films via selenization at 700°C in a selenium-rich low-pressure environment ($\sim 10^{-3}$ torr base pressure) in contrast to atmospheric pressure selenization process. [A5]

Author's publication list

Publications related to this work:

A1 – Butanovs, E., **Kadiwala, K**., Gopejenko, A., Bocharov, D., Piskunov, S. & Polyakov, B. Different strategies for GaN-MoS_2 and GaN-WS_2 core–shell nanowire growth. Appl Surf Sci 590, (2022).

A2 – Polyakov, B., **Kadiwala, K**., Butanovs, E., Dipane, L., Trausa, A., Bocharov, D. & Vlassov, S. Synthesis of ZnS/Al_2O_3/Ta_Se_2 Core/Shell Nanowires Using Thin Ta Metal Film Precursor. ChemEngineering 8, (2024).

A3 – **Kadiwala, K**., Butanovs, E., Ogurcovs, A., Zubkins, M. & Polyakov, B. Comparative study of WSe_2 thin films synthesized via pre-deposited WO_3 and W precursor material selenization. J Crystal Growth 593, (2022).

A4 – **Kadiwala, K.**, Dipane, L., Dipans, E., Bundulis, A., Zubkins, M., Ogurcovs, A., Gabrusenoks, J., Bocharov, D., Butanovs, E. & Polyakov, B. Synthesis and investigation of $ReSe_2$ Thin Films Derived from Magnetron Sputtered Re and ReO_x. Crystals 14, (2024).

A5 – **Kadiwala, K.**, Dipans, E., Dipane, L., Butanovs, E. & Polyakov, B. Towards Scalable Synthesis of $TiSe_2$ and VSe_2 Thin Films. Latvian Journal of Physics and Technical Sciences 61, 13–22 (2024).

Author's other publications:

B1 - Ogurcovs, A., **Kadiwala, K.**, Sledevskis, E., Krasovska, M. & Mizers, V. Glyphosate Sensor Based on Nanostructured Water-Gated CuO Field-Effect Transistor. Sensors 22, 8744 (2022).

B2 - Ogurcovs, A., **Kadiwala, K.**, Sledevskis, E., Krasovska, M., Plaksenkova, I. & Butanovs, E. Effect of DNA Aptamer Concentration on the Conductivity of a Water-Gated Al:ZnO Thin-Film Transistor-Based Biosensor. Sensors 22, 3408 (2022).

B3 - Polyakov, B., Novikovs, A., Leimane, M., **Kadiwala, K.**, Zubkins, M., Butanovs, E., Oras, S., Damerchi, E., Zadin, V. & Vlassov, S. Comparison of the resistivities of nanostructured films made from silver, copper-silver and copper nanoparticle and nanowire suspensions. Thin Solid Films 784, 140087 (2023).

B4 - Butanovs E., Zubkins M., Strods E., Vibornijs V., **Kadiwala K.**, Ignatane L., Polyakov B., Vlassov S., Purans J., Impact of temperature and film thickness on α- and β- phase formation in Ga_2O_3 thin films grown on a-plane sapphire substrate, Thin Solid Films, Volume 803,2024,140467 (2024).

Author's contribution in listed publications:

A1 - Data visualization, material synthesis (PLD experiments – Shell on nanowires)

A2 - Data visualization, material synthesis (Nanowire synthesis- Core and Shell), XRD measurements.

A3 - Corresponding author, body of the article written, material synthesis (CVD synthesis), SEM, XRD measurements, device fabrication (Optical Lithography) and characterization.

A4 - Corresponding author, body of the article written, material synthesis (Magnetron Sputtering, CVD synthesis), SEM, XRD measurements and data analysis and visualization.

A5 - Corresponding author, body of the article written, material synthesis (Magnetron Sputtering, CVD synthesis), Optical images, SEM, XRD measurements and data analysis.

Participation in schools and conferences

PhD Schools

1. CAMART2 Remote Summer School [sept 2021, online]
2. COST - International Training school Modern directions in Epitaxy [June2022, Denmark]
3. FORTHEM – 'Escola d'Estiu Erasmus de Fisica' mobility program [July 2022, Spain]
4. European School on Nanosciences and Nanotechnologies [Aug 2022, France]
5. International Winterschool on Electronic Properties of Novel Materials [March 2023, Austria]

Conferences

1. ISSP UL 37th Scientific Conferences – [Presentation: Bottom-up synthesis of tungsten diselenide thin films and electric contact fabrication - Kevon Kadiwala, Edgars Butanovs, Martins Zubkins, Boris Polyakov] [Feb 2021, online]
2. ISSP UL 38th Scientific Conferences – [Presentation: Synthesis and characterization of 2D crystals and nanowires for the fabrication of heterojunctions - Kevon Kadiwala, Edgars Butanovs, Andrejs Ogurcovs, Boris Polyakov] [Feb 2022, Latvia]
3. Physics and Natural sciences - Open Readings – [Poster: WSe_2 thin films comparison synthesized via pre-deposited WO_3 and W precursor material selenization - Kevon Kadiwala, Edgars Butanovs, Andrejs Ogurcovs, Martins Zubkins, Boris Polyakov] [March 2022, online]
4. European Materials Research Society (E-MRS) – [Presentation: Comparative study of WSe_2 thin films synthesized via pre-deposited WO_3 and W precursor material selenization - Kevon Kadiwala, Edgars

Butanovs, Andrejs Ogurcovs, Martins Zubkins, Boris Polyakov] [May 2022, online]

5. Functional materials and Nanotechnologies (FMNT) – [Poster: Thin films of WSe_2 synthesized via selenization of WO_3 and W precursor materials for characteristic comparison - Kevon Kadiwala, Edgars Butanovs, Andrejs Ogurcovs, Martins Zubkins, Boris Polyakov] [July 2022, Latvia]

6. Advanced Materials and Technologies conference (AMT) – [Poster: Characteristic assessment of WSe_2 thin films synthesized from W and WO3 precursor materials - Kevon Kadiwala, Edgars Butanovs, Andrejs Ogurcovs, Martins Zubkins, Boris Polyakov] [Aug 2022, Lithuania]

7. ISSP UL 39th Scientific Conferences – [Presentation: Different strategies for GaN-MoS_2 and GaN-WS_2 core–shell nanowire growth – Edgars Butanovs, Kevon Kadiwala, Aleksejs Gopejenko, Dmitry Bocharov, Sergei Piskunov, Boris Polyakov] [March 2023, Latvia]

8. ISSP UL 40th Scientific Conferences – [Presentation: Synthesis and investigation of $ReSe_2$ Thin Films Derived from Magnetron Sputtered Re and ReOx – Kevon Kadiwala, Luize Dipane, Eriks Dipans, Arturs Bundulis, Martins Zubkins, Andrejs Ogurcovs, Jevgenijs Gabrusenoks, Dmitry Bocharov, Edgars Butanovs, Boris Polyakov] [March 2024, Latvia]

References

[1] J.D. Cain, E.D. Hanson, F. Shi, V.P. Dravid, Emerging opportunities in the two-dimensional chalcogenide systems and architecture, Curr Opin Solid State Mater Sci 20 (2016) 374–387. https://doi.org/10.1016/j.cossms.2016.06.001.

[2] P. Wang, Y. Yang, E. Pan, F. Liu, P.M. Ajayan, J. Zhou, Z. Liu, Emerging Phases of Layered Metal Chalcogenides, Small 18 (2022). https://doi.org/10.1002/smll.202105215.

[3] Y. Liu, N.O. Weiss, X. Duan, H.-C. Cheng, Y. Huang, X. Duan, Van der Waals heterostructures and devices, Nat Rev Mater 1 (2016) 16042. https://doi.org/10.1038/natrevmats.2016.42.

[4] A. McCreary, O. Kazakova, D. Jariwala, Z.Y. Al Balushi, An outlook into the flat land of 2D materials beyond graphene: synthesis, properties and device applications, 2d Mater 8 (2021) 013001. https://doi.org/10.1088/2053-1583/abc13d.

[5] S. Jain, R. Trivedi, J.K. Banshiwal, A.S. Singh, B. Chakraborty, Two-dimensional materials (2DMs): classification, preparations, functionalization and fabrication of 2DMs-oriented electrochemical sensors, in: 2D Materials-Based Electrochemical Sensors, Elsevier, 2023: pp. 45–132. https://doi.org/10.1016/B978-0-443-15293-1.00005-7.

[6] Y. Fu, Y. Liao, P. Li, H. Li, S. Jiang, H. Huang, W. Sun, T. Li, H. Yu, K. Li, H. Li, B. Jia, T. Ma, Layer structured materials for ambient nitrogen fixation, Coord Chem Rev 460 (2022) 214468. https://doi.org/10.1016/j.ccr.2022.214468.

[7] C. Tan, Z. Lai, H. Zhang, Ultrathin Two-Dimensional Multinary Layered Metal Chalcogenide Nanomaterials, Advanced Materials 29 (2017). https://doi.org/10.1002/adma.201701392.

[8] A. Majid, A. Jabeen, Transition Metal Dichalcogenides—An Important Class of Layered Materials, in: 2023: pp. 103–140. https://doi.org/10.1007/978-981-99-6299-0_5.

[9] X. Chia, Exploring layered metal chalcogenides : electrochemistry and application, Nanyang Technological University, 2018. https://doi.org/10.32657/10220/47379.

[10] J.J. Heath, M.A. Kuroda, Spin-Injection Enhancements in van der Waals Magnetic Tunnel Junctions through Barrier Engineering, Phys Rev Appl 16 (2021) L041001. https://doi.org/10.1103/PhysRevApplied.16.L041001.

[11] G. Ghimire, K.P. Dhakal, W. Choi, Y.A. Esthete, S.J. Kim, T.T. Tran, H. Lee, H. Yang, D.L. Duong, Y.-M. Kim, J. Kim, Doping-Mediated Lattice Engineering of Monolayer ReS_2 for Modulating In-Plane Anisotropy of Optical and Transport Properties, ACS Nano 15 (2021) 13770–13780. https://doi.org/10.1021/acsnano.1c05316.

[12] R. Roldán, A. Castellanos-Gomez, E. Cappelluti, F. Guinea, Strain engineering in semiconducting two-dimensional crystals, Journal of Physics: Condensed Matter 27 (2015) 313201. https://doi.org/10.1088/0953-8984/27/31/313201.

[13] J.H. Kim, H. Sung, G.-H. Lee, Phase Engineering of Two-Dimensional Transition Metal Dichalcogenides, Small Science 4 (2024). https://doi.org/10.1002/smsc.202300093.

[14] F. Yang, P. Song, M. Ruan, W. Xu, Recent progress in two-dimensional nanomaterials: Synthesis, engineering, and applications, FlatChem 18 (2019) 100133. https://doi.org/10.1016/j.flatc.2019.100133.

[15] L.M. Xie, Two-dimensional transition metal dichalcogenide alloys: preparation, characterization and applications, Nanoscale 7 (2015) 18392–18401. https://doi.org/10.1039/C5NR05712D.

[16] H. Li, Y. Shi, M.-H. Chiu, L.-J. Li, Emerging energy applications of two-dimensional layered transition metal dichalcogenides, Nano Energy 18 (2015) 293–305. https://doi.org/10.1016/j.nanoen.2015.10.023.

[17] Y. Zhao, Y. Yan, J.-M. Lee, Recent progress on transition metal diselenides from formation and modification to applications, Nanoscale 14 (2022) 1075–1095. https://doi.org/10.1039/D1NR07789A.

[18] W. Chen, E.J.G. Santos, W. Zhu, E. Kaxiras, Z. Zhang, Tuning the Electronic and Chemical Properties of Monolayer MoS_2 Adsorbed on Transition Metal Substrates, Nano Lett 13 (2013) 509–514. https://doi.org/10.1021/nl303909f.

[19] K.K. Pawar, A. Kumar, A. Mirzaei, M. Kumar, H.W. Kim, S.S. Kim, 2D nanomaterials for realization of flexible and wearable gas sensors: A review, Chemosphere 352 (2024) 141234. https://doi.org/10.1016/j.chemosphere.2024.141234.

[20] B. Radisavljevic, A. Radenovic, J. Brivio, V. Giacometti, A. Kis, Single-layer MoS2 transistors, Nat Nanotechnol 6 (2011) 147–150. https://doi.org/10.1038/nnano.2010.279.

[21] D. Lembke, S. Bertolazzi, A. Kis, Single-Layer MoS_2 Electronics, Acc Chem Res 48 (2015) 100–110. https://doi.org/10.1021/ar500274q.

[22] Q.H. Wang, K. Kalantar-Zadeh, A. Kis, J.N. Coleman, M.S. Strano, Electronics and optoelectronics of two-dimensional transition metal dichalcogenides, Nat Nanotechnol 7 (2012) 699–712. https://doi.org/10.1038/nnano.2012.193.

[23] A. Diebold, T. Hofmann, Optical and Electrical Properties of Transition Metal Dichalcogenides (Monolayer and Bulk), in: 2021: pp. 295–361. https://doi.org/10.1007/978-3-030-80323-0_8.

[24] J. Cao, Y. Zhang, C. Zhang, L. Cai, Z. Li, C. Zhou, Construction of defect-rich 1T-MoS2 towards efficient electrocatalytic hydrogen evolution: Recent advances and future perspectives, Surfaces and Interfaces 25 (2021) 101305. https://doi.org/10.1016/j.surfin.2021.101305.

[25] A. Sinha, Dhanjai, B. Tan, Y. Huang, H. Zhao, X. Dang, J. Chen, R. Jain, MoS2 nanostructures for electrochemical sensing of multidisciplinary targets: A review, TrAC Trends in Analytical Chemistry 102 (2018) 75–90. https://doi.org/10.1016/j.trac.2018.01.008.

[26] J.M. Vandenberg-Voorhoeve, Structural and Magnetic Properties of Layered Chalcogenides of the Transition Elements, in: Optical and Electrical Properties, Springer Netherlands, Dordrecht, 1976: pp. 423–457. https://doi.org/10.1007/978-94-010-1478-6_8.

[27] A. Taffelli, S. Dirè, A. Quaranta, L. Pancheri, MoS2 Based Photodetectors: A Review, Sensors 21 (2021) 2758. https://doi.org/10.3390/s21082758.

[28] S. Kim, All-2D material photonic devices, Nanoscale Adv 5 (2023) 323–328. https://doi.org/10.1039/D2NA00732K.

[29] F. Yan, C. Hu, Z. Wang, H. Lin, K. Wang, Perspectives on photodetectors based on selenides and their van der Waals heterojunctions, Appl Phys Lett 118 (2021). https://doi.org/10.1063/5.0045941.

[30] A. Pal, S. Zhang, T. Chavan, K. Agashiwala, C. Yeh, W. Cao, K. Banerjee, Quantum-Engineered Devices Based on 2D Materials for Next-Generation Information Processing and Storage, Advanced Materials 35 (2023). https://doi.org/10.1002/adma.202109894.

[31] M. Brotons-Gisbert, B.D. Gerardot, Quantum Photonics with 2D Semiconductors, in: Photonic Quantum Technologies, Wiley, 2023: pp. 563–579. https://doi.org/10.1002/9783527837427.ch20.

[32] M. Turunen, M. Brotons-Gisbert, Y. Dai, Y. Wang, E. Scerri, C. Bonato, K.D. Jöns, Z. Sun, B.D. Gerardot, Quantum photonics with layered 2D materials, Nature Reviews Physics 4 (2022) 219–236. https://doi.org/10.1038/s42254-021-00408-0.

[33] A. Reserbat-Plantey, I. Epstein, I. Torre, A.T. Costa, P.A.D. Gonçalves, N.A. Mortensen, M. Polini, J.C.W. Song, N.M.R. Peres, F.H.L. Koppens, Quantum Nanophotonics in Two-Dimensional Materials, ACS Photonics 8 (2021) 85–101. https://doi.org/10.1021/acsphotonics.0c01224.

[34] M. Kianinia, Z.-Q. Xu, M. Toth, I. Aharonovich, Quantum emitters in 2D materials: Emitter engineering, photophysics, and integration in photonic nanostructures, Appl Phys Rev 9 (2022). https://doi.org/10.1063/5.0072091.

[35] G.S. Lee, J.G. Kim, J.T. Kim, C.W. Lee, S. Cha, G.B. Choi, J. Lim, S. Padmajan Sasikala, S.O. Kim, 2D Materials Beyond Post-AI Era: Smart Fibers, Soft Robotics, and Single Atom Catalysts, Advanced Materials 36 (2024). https://doi.org/10.1002/adma.202307689.

[36] Y.-T. Guo, S.-S. Yi, Recent Advances in the Preparation and Application of Two-Dimensional Nanomaterials, Materials 16 (2023) 5798. https://doi.org/10.3390/ma16175798.

[37] Y. Jung, J. Shen, J.J. Cha, Surface effects on electronic transport of 2D chalcogenide thin films and nanostructures, Nano Converg 1 (2014) 18. https://doi.org/10.1186/s40580-014-0018-2.

[38] D.M. Soares, S. Mukherjee, G. Singh, TMDs beyond MoS_2 for Electrochemical Energy Storage, Chemistry – A European Journal 26 (2020) 6320–6341. https://doi.org/10.1002/chem.202000147.

[39] X. Wu, M. Sun, H. Yu, B. Huang, Z.L. Wang, Unraveling the unique response behaviors of ultrathin transition metal dichalcogenides to external excitations, Nano Energy 115 (2023) 108721. https://doi.org/10.1016/j.nanoen.2023.108721.

[40] S. Noreen, M.B. Tahir, A. Hussain, T. Nawaz, J.U. Rehman, A. Dahshan, M. Alzaid, H. Alrobei, Emerging 2D-Nanostructured materials for electrochemical and sensing Application-A review, Int J Hydrogen Energy 47 (2022) 1371–1389. https://doi.org/10.1016/j.ijhydene.2021.10.044.

[41] Z. Huo, Y. Wei, Y. Wang, Z.L. Wang, Q. Sun, Integrated Self-Powered Sensors Based on 2D Material Devices, Adv Funct Mater 32 (2022). https://doi.org/10.1002/adfm.202206900.

[42] J.H. Appel, D.O. Li, J.D. Podlevsky, A. Debnath, A.A. Green, Q.H. Wang, J. Chae, Low Cytotoxicity and Genotoxicity of Two-Dimensional MoS_2 and WS_2, ACS Biomater Sci Eng 2 (2016) 361–367. https://doi.org/10.1021/acsbiomaterials.5b00467.

[43] P. Karfa, K. Chandra Majhi, R. Madhuri, Synthesis of two-dimensional nanomaterials, in: Two-Dimensional Nanostructures for Biomedical Technology, Elsevier, 2020: pp. 35–71. https://doi.org/10.1016/B978-0-12-817650-4.00002-4.

[44] M. Ahmadi, O. Zabihi, S. Jeon, M. Yoonessi, A. Dasari, S. Ramakrishna, M. Naebe, 2D transition metal dichalcogenide nanomaterials: advances, opportunities, and challenges in multi-

functional polymer nanocomposites, J Mater Chem A Mater 8 (2020) 845–883. https://doi.org/10.1039/C9TA10130F.

[45] T.F. Schranghamer, M. Sharma, R. Singh, S. Das, Review and comparison of layer transfer methods for two-dimensional materials for emerging applications, Chem Soc Rev 50 (2021) 11032–11054. https://doi.org/10.1039/D1CS00706H.

[46] Y. Chang, N. Yang, J. Min, F. Zheng, C. Huang, J. Chen, Y. Zhang, P. Yang, C. Li, H. Liu, B. Ye, J. Xu, H. Chen, Z. Luo, W. Wu, K. Shih, J. Huang, L. Li, Y. Wan, Atomically Thin Decoration Layers for Robust Orientation Control of 2D Transition Metal Dichalcogenides, Adv Funct Mater 34 (2024). https://doi.org/10.1002/adfm.202311387.

[47] C. Tan, X. Cao, X.-J. Wu, Q. He, J. Yang, X. Zhang, J. Chen, W. Zhao, S. Han, G.-H. Nam, M. Sindoro, H. Zhang, Recent Advances in Ultrathin Two-Dimensional Nanomaterials, Chem Rev 117 (2017) 6225–6331. https://doi.org/10.1021/acs.chemrev.6b00558.

[48] Y. Yi, Z. Chen, X. Yu, Z. Zhou, J. Li, Recent Advances in Quantum Effects of 2D Materials, Adv Quantum Technol 2 (2019). https://doi.org/10.1002/qute.201800111.

[49] H.H. Huang, X. Fan, D.J. Singh, W.T. Zheng, Recent progress of TMD nanomaterials: phase transitions and applications, Nanoscale 12 (2020) 1247–1268. https://doi.org/10.1039/C9NR08313H.

[50] K. Khan, A.K. Tareen, M. Aslam, R. Wang, Y. Zhang, A. Mahmood, Z. Ouyang, H. Zhang, Z. Guo, Recent developments in emerging two-dimensional materials and their applications, J Mater Chem C Mater 8 (2020) 387–440. https://doi.org/10.1039/C9TC04187G.

[51] Z. Zheng, T. Zhang, J. Yao, Y. Zhang, J. Xu, G. Yang, Flexible, transparent and ultra-broadband photodetector based on large-area WSe2 film for wearable devices, Nanotechnology 27 (2016) 1–11. https://doi.org/10.1088/0957-4484/27/22/225501.

[52] J. Ding, A. Feng, X. Li, S. Ding, L. Liu, W. Ren, Properties, preparation, and application of tungsten disulfide: a review, J Phys D Appl Phys 54 (2021) 173002. https://doi.org/10.1088/1361-6463/abd9e8.

[53] J.H. Han, M. Kwak, Y. Kim, J. Cheon, Recent Advances in the Solution-Based Preparation of Two-Dimensional Layered Transition Metal Chalcogenide Nanostructures, Chem Rev 118 (2018) 6151–6188. https://doi.org/10.1021/acs.chemrev.8b00264.

[54] M. Chhowalla, Z. Liu, H. Zhang, Two-dimensional transition metal dichalcogenide (TMD) nanosheets, Chem Soc Rev 44 (2015) 2584–2586. https://doi.org/10.1039/C5CS90037A.

[55] S. Yu, Q. Rice, B. Tabibi, Q. Li, F.J. Seo, Piezoelectricity in WSe2/MoS2 heterostructure atomic layers, Nanoscale 10 (2018) 12472–12479. https://doi.org/10.1039/c8nr04394a.

[56] C. Huang, S. Wu, A.M. Sanchez, J.J.P. Peters, R. Beanland, J.S. Ross, P. Rivera, W. Yao, D.H. Cobden, X. Xu, Lateral heterojunctions within monolayer MoSe2-WSe2 semiconductors, Nat Mater 13 (2014) 1096–1101. https://doi.org/10.1038/nmat4064.

[57] A.K. Geim, I. V. Grigorieva, Van der Waals heterostructures, Nature 499 (2013) 419–425. https://doi.org/10.1038/nature12385.

[58] P. Lin, J. Yang, Tunable WSe2/WS2 van der Waals heterojunction for self-powered photodetector and photovoltaics, J Alloys Compd 842 (2020) 155890. https://doi.org/10.1016/j.jallcom.2020.155890.

[59] N.A. Shepelin, Z.P. Tehrani, N. Ohannessian, C.W. Schneider, D. Pergolesi, T. Lippert, A practical guide to pulsed laser deposition, Chem Soc Rev 52 (2023) 2294–2321. https://doi.org/10.1039/D2CS00938B.

[60] M.J. Aziz, Film growth mechanisms in pulsed laser deposition, Applied Physics A 93 (2008) 579–587. https://doi.org/10.1007/s00339-008-4696-7.

[61] J. Musil, P. Baroch, J. Vlček, K.H. Nam, J.G. Han, Reactive magnetron sputtering of thin films: present status and trends, Thin Solid Films 475 (2005) 208–218. https://doi.org/10.1016/j.tsf.2004.07.041.

[62] S.M. Rossnagel, Magnetron sputtering, Journal of Vacuum Science & Technology A: Vacuum, Surfaces, and Films 38 (2020). https://doi.org/10.1116/6.0000594.

[63] Y. Shi, H. Li, L.-J. Li, Recent advances in controlled synthesis of two-dimensional transition metal dichalcogenides via vapour deposition techniques, Chem Soc Rev 44 (2015) 2744–2756. https://doi.org/10.1039/C4CS00256C.

[64] L. Sun, G. Yuan, L. Gao, J. Yang, M. Chhowalla, M.H. Gharahcheshmeh, K.K. Gleason, Y.S. Choi, B.H. Hong, Z. Liu, Chemical vapour deposition, Nature Reviews Methods Primers 1 (2021) 5. https://doi.org/10.1038/s43586-020-00005-y.

[65] R.K. Crouch, W.J. Debnam, R. Ryan, Vacuum tight quartz ampoule for bridgman growth of crystals with interface demarcation, J Cryst Growth 56 (1982) 215–216. https://doi.org/10.1016/0022-0248(82)90031-8.

[66] J. Lee, H. Jang, T. Kwak, U. Choi, B. So, O. Nam, Growth and characterization of MoS2/n-GaN and MoS2/p-GaN vertical heterostructure with wafer scale homogeneity, Solid State Electron 165 (2020) 107751. https://doi.org/10.1016/j.sse.2019.107751.

[67] S.E. Panasci, I. Deretzis, E. Schilirò, A. La Magna, F. Roccaforte, A. Koos, M. Nemeth, B. Pécz, M. Cannas, S. Agnello, F. Giannazzo, Interface Properties of MoS2 van der Waals Heterojunctions with GaN, Nanomaterials 14 (2024) 133. https://doi.org/10.3390/nano14020133.

[68] F. Khan, M. Idrees, C. Nguyen, I. Ahmad, B. Amin, A first-principles study of electronic structure and photocatalytic performance of GaN–MX2 (M = Mo, W; X= S, Se) van der Waals heterostructures, RSC Adv 10 (2020) 24683–24690. https://doi.org/10.1039/D0RA04082G.

[69] E. Hossain, A.A. Rahman, A.P. Shah, B.A. Chalke, A. Bhattacharya, Large-area, thermally-sulfurized WS2 thin films: control of growth direction and use as a substrate for GaN epitaxy, Semicond Sci Technol 35 (2020) 035011. https://doi.org/10.1088/1361-6641/ab6bb3.

[70] Z. Yan, C. Jiang, T.R. Pope, C.F. Tsang, J.L. Stickney, P. Goli, J. Renteria, T.T. Salguero, A.A. Balandin, Phonon and thermal properties of exfoliated TaSe2 thin films, J Appl Phys 114 (2013). https://doi.org/10.1063/1.4833250.

[71] Y. Wu, J. He, J. Liu, H. Xing, Z. Mao, Y. Liu, Dimensional reduction and ionic gating induced enhancement of superconductivity in atomically thin crystals of 2H-TaSe2, Nanotechnology 30 (2019) 035702. https://doi.org/10.1088/1361-6528/aaea3b.

[72] P. Zhou, P. Schiettecatte, M. Vandichel, A. Rousaki, P. Vandenabeele, Z. Hens, S. Singh, Synthesis of Colloidal WSe2Nanocrystals: Polymorphism Control by Precursor-Ligand Chemistry, Cryst Growth Des 21 (2021) 1451–1460. https://doi.org/10.1021/acs.cgd.0c01036.

[73] Z. Wang, H.H. Wu, Q. Li, F. Besenbacher, Y. Li, X.C. Zeng, M. Dong, Reversing Interfacial Catalysis of Ambipolar WSe2 Single Crystal, Advanced Science 7 (2020). https://doi.org/10.1002/advs.201901382.

[74] G. Clark, S. Wu, P. Rivera, J. Finney, P. Nguyen, D.H. Cobden, X. Xu, Vapor-transport growth of high optical quality WSe2 monolayers, APL Mater 2 (2014). https://doi.org/10.1063/1.4896591.

[75] Y. Mao, H. Wang, I. Kislyakov, Z. Wang, N. Dong, J. Wang, Nonlinear optical properties and ultrafast carrier dynamics of ultrathin ReSe2, Opt Lett 48 (2023) 6259. https://doi.org/10.1364/OL.510204.

[76] B. Silva, J. Rodrigues, B. Sompalle, C.-D. Liao, N. Nicoara, J. Borme, F. Cerqueira, M. Claro, S. Sadewasser, P. Alpuim, A. Capasso, Efficient ReSe2 Photodetectors with CVD Single-Crystal Graphene Contacts, Nanomaterials 11 (2021) 1650. https://doi.org/10.3390/nano11071650.

[77] A. Pandey, R. Verma, A. Srivastava, Two-dimensional ReSe2 nanosheets as a high-performance photocatalyst, New Journal of Chemistry 47 (2023) 12983–12991. https://doi.org/10.1039/D3NJ01440A.

[78] A. Feroze, H.R. Na, Y.C. Park, J.-H. Jun, M.-H. Jung, J.-H. Lee, J.-H. Kim, M.-J. Seong, S. Hong, S.-H. Chun, S. Lee, In-Depth Structural Characterization of 1T-VSe2 Single Crystals Grown by Chemical Vapor Transport, Cryst Growth Des 20 (2020) 2860–2865. https://doi.org/10.1021/acs.cgd.0c00219.

[79] S. Das, N. Mohapatra, Tunable Physical Properties of VSe2 hexagonal disks, J Phys Conf Ser 2518 (2023) 012010. https://doi.org/10.1088/1742-6596/2518/1/012010.

[80] A. Jain, S.P. Ong, G. Hautier, W. Chen, W.D. Richards, S. Dacek, S. Cholia, D. Gunter, D. Skinner, G. Ceder, K.A. Persson, Commentary: The Materials Project: A materials genome approach to accelerating materials innovation, APL Mater 1 (2013). https://doi.org/10.1063/1.4812323.

Acknowledgements

First and foremost, I would like to express my sincere gratitude to my supervisor, Dr. Boris Polyakovs, for his vital guidance and support throughout my PhD studies. His overall expertise in the field of material science and his dedication to my development have been instrumental in shaping my research journey.

Special thanks goes to Dr. Edgars Butanovs for his significant contributions to my research. His invaluable guidance, from the very beginning of teaching me experimental tools, methodologies and to instilling the importance of adaptability in this field, has been instrumental to my success.

I am indebted to my colleagues for their support and camaraderie throughout my research. Their insights, experimental support, and guidance were essential to the success of my research. I would like to express my sincere appreciation to Andrejs Ogurcovs, Martin Zubkins, Annamarija Trausa, Karlis Vilks, Arturs Bundulis, Aleksejs Zoltrovs, Alexei Kuzmins, Liga Jasulaneca, Luize Dipane, Eriks Dipans, Viktors Vibornijs, Edwards Strods, Alexanders Novikovs, Thomas Yager, and Halil Arslan.

I extend my sincere thanks to Juris Purans, Andris Anspoks, and Andris Sternbergs for their committed belief in my abilities and their generous financial support. Their contributions have been instrumental in creating an environment that allowed me to fully concentrate on my research.

Finally, I would like to express my sincere gratitude to my family and friends for their unwavering support throughout my PhD journey. My brother's constant encouragement has been a source of inspiration for me. I am eternally grateful to my dearest friend, Nair, whose belief in me made this entire journey possible. I would also like to acknowledge the invaluable support of my Dostaar, my Luvvo and Don Pablo whose encouragement and discussions have been instrumental in my success.

I am grateful for the financial support provided by the Latvian Council of Science through projects LZP-2020/1-0261 and LZP-2020/1-0345. Furthermore, the Institute of Solid State Physics, University of Latvia, awarded two 'Student and Young Researcher Grants' to support this research. Additionally, the European Union's Horizon 2020 Framework Programme grant CAMART2 (No. 739508) played a crucial role in enhancing the quality and scope of the study.